The combined exact diagonalization–*ab initio* approach and its application to correlated electronic states and Mott–Hubbard localization in nanoscopic systems

2007 J. Phys.: Condens. Matter 19 255212

(http://iopscience.iop.org/0953-8984/19/25/255212)

IOP PUBLISHING JOURNAL OF PHYSICS: CONDENSED MATTER

J. Phys.: Condens. Matter **19** (2007) 255212 (43pp) doi:10.1088/0953-8984/19/25/255212

The combined exact diagonalization–*ab initio* approach and its application to correlated electronic states and Mott–Hubbard localization in nanoscopic systems

Jozef Spałek, Edward M Görlich, Adam Rycerz and Roman Zahorbeński

Marian Smoluchowski Institute of Physics, Jagiellonian University, ulica Reymonta 4, 30-059 Kraków, Poland

Received 27 October 2006, in final form 14 November 2006
Published 30 May 2007
Online at stacks.iop.org/JPhysCM/19/255212

Abstract

We overview the EDABI method developed recently combining the exact diagonalization and *ab initio* aspects of electron states in correlated systems and apply it to nanoscopic systems. In particular, we discuss the localization–delocalization transition for the electrons that corresponds to the Mott–Hubbard transition in bulk systems. We show that the statistical distribution function for electrons in a nanochain evolves from Fermi–Dirac-like to Luttinger-liquid-like with the increasing interatomic distance. The concept of Hubbard subbands is introduced to nanoclusters, and corresponds to the HOMO–LUMO splitting in the molecular and organic solid states. Also, the nanochains exhibit magnetic splitting (Slater-like), even without the symmetry breaking, since the spin–spin correlations extend over the whole system. Thus, the correlated nanoscopic systems exhibit unique and universal features, which differ from those of molecular and infinite systems. These features define unique properties reflecting '*the Mott physics*' on the nanoscale. We also employ the EDABI method for the transport properties in nanoscopic systems. For example, we show that the particle–hole symmetry is broken when the tunnelling conduction through the H_2 molecule is calculated.

(Some figures in this article are in colour only in the electronic version)

1. Introduction

The studies of *nanosystems* are becoming increasingly important in view of their application in quantum nanoelectronics and related fields of research. Of particular importance are their quantum electronic properties, since they determine their behaviour as concrete devices: quantum nanowire connectors and semiconducting elements, single-electron transistors, spin valves etc. Under these circumstances, solid-state and molecular *nanophysics* is developing very rapidly to provide proper quantitative (and qualitative) characteristics of their static, transport, and optical properties [1].

Independently of the applications, the research in *nanophysics* is important for its own fundamental sake. Namely, the nanosystems are finite systems and therefore most of the limiting situations considered in the condensed matter physics and involving the limit for the number of atoms $N \to \infty$ are simply inapplicable. Furthermore, the role of boundary conditions is very nontrivial, as they should reflect the system actual configuration. Also, and probably most importantly, the question of electron–electron interactions, particularly for extended states, should be taken into account on equal footing with the single-electron aspects of their quantum states, since the screening processes are very often highly ineffective. Nevertheless, given the circumstances, the role of physics is to single out universal properties of the systems such as nanowires, clusters, quantum dots, etc. Such research also involves determining the conditions under which the bulk-solid concepts are applicable, since then the description can be simplified remarkably.

In this paper we present our recent and earlier results concerning the studies of nanosystems containing as an intrinsic property the electron correlation effects induced by the Coulomb interactions, within the devised EDABI method combining both exact diagonalization and *ab initio* aspects of electronic states, as well as their transport properties [2]. This approach allows for discussion of the evolution of the physical properties of e.g. nanowires or clusters, both as a function of their interatomic distance as well as to determine the values of microscopic single-particle and interaction parameters. The visualization of the properties as a function of interatomic distance is particularly important for nanometre size systems, as they are studied customarily by placing them on a substrate with the lattice parameter, which differs from their equilibrium interatomic distance (sometimes the substrate even stabilizes them).

Our most interesting results can be summarized as follows. First, we show how the system properties evolve from the Fermi-liquid-like to the atomic-like states for nanowires containing up to $N = 16$ simple atoms, passing through the Luttinger-liquid-like state, with the increasing interatomic distance R. This evolution is determined by calculating directly the system statistical distribution function $n_{k\sigma}$ of electrons and their dynamical spectral function. Finite-size scaling properties are introduced to determine the *Mott critical interatomic distance (the Mott criterion)* for the transition from the delocalized to the localized states. Second, we show that the electronic states in nanosystems of $N \sim 10$ atoms exhibit a magnetic splitting reminiscent of the *Slater splitting* in antiferromagnetic metallic systems [3]. This type of symmetry change is associated with the breakdown of the discrete translational symmetry, as the antiferromagnetism sets in. In the case of nanosystems such symmetry breakdown is not required. It turns out that the splitting appears if the spin–spin correlation length is of the system size. The splitting should be detected e.g. in nanowires containing strongly correlated electrons in a half-filled valence band configuration. Third, the question arises of whether with the increasing interatomic distance one should not observe the Hubbard split-band structure of nanowire and molecular (e.g. H_N or Li_N) clusters. We show that nanocluster levels group into multiple Hubbard subbands (in bulk systems such a grouping is termed HOMO and LUMO structures). Finally, in the case of a quantum dot composed of e.g. an H_2 molecule attached to the semimacroscopic electrodes we show that the electron–hole symmetry in the tunnelling transport through the molecule is not preserved and is due to the difference in electronic binding energy of H_2^+ and H_2^- states. Such result is not obtained if a parametrized model of a quantum dot properties is used [4].

The structure of this paper is as follows. In the next section we overview the EDABI method [3–7], as well as discussing some of the many-electron general properties adopted for the analysis carried out in the next sections. We also compare the method with the configuration interaction (CI) approach used in quantum chemistry. In section 3 we discuss atomic systems and H_N nanoclusters, whereas in section 4 the results for nanochains containing up to $N = 16$

atoms are elaborated in detail. In section 5 we employ the EDABI method to calculate the tunnelling conductivity through the H_2 molecule and the Drude weight for the nanochains. We also discuss the role of boundary conditions there.

The present method and the research grew out of our earlier work on the thermodynamics of the Mott–Hubbard transition in correlated systems [8]. There, the principal question was whether the metallic and magnetic insulating states can be regarded as separate phases in the thermodynamic sense. The affirmative answer to the above question provided a partial answer to Sir Nevill Mott's question: *What is a metal?* In this paper the corresponding principal question is *how small can a piece of metal be?* In other words, can a nanochain composed of e.g. $N = 10$ Cu atoms be regarded already as a metallic system and in what sense? The answer is 'yes', but above a critical value of voltage applied to the chain and for not too large interatomic distance.

2. Exact diagonalization combined with an *ab initio* approach

2.1. General features

The second-quantization language is used when we have an interaction between the quantum physical fields representing the classical particles composing the system. The approach is usually formulated in the occupation-number representation, expressing the possible occupations of a given (*complete* in the quantum mechanical sense) set of single-particle states, between which there are transitions induced by their mutual interaction. Explicitly, the single-particle basis $\{\Phi_i(\mathbf{r})\}$ defines the field operator $\hat{\Psi}(\mathbf{r})$, in terms of which the many-particle Hamiltonian (or Lagrangian) is defined. In the nonrelativistic case, the Hamiltonian is defined as [9]

$$\hat{H} = \int \mathrm{d}^3\mathbf{r}\hat{\Psi}^\dagger(\mathbf{r})H_1(\mathbf{r})\hat{\Psi}(\mathbf{r}) + \tfrac{1}{2}\int \mathrm{d}^3r\,\mathrm{d}^3r'\hat{\Psi}^\dagger(\mathbf{r})\hat{\Psi}^\dagger(\mathbf{r}')V(\mathbf{r}-\mathbf{r}')\hat{\Psi}(\mathbf{r}')\hat{\Psi}(\mathbf{r}) \equiv \hat{T} + \hat{V} \tag{1}$$

with

$$\hat{\Psi}(\mathbf{r}) = \sum_i \Phi_i(\mathbf{r})a_i. \tag{2}$$

$H_1(\mathbf{r})$ represents the Hamiltonian for a single particle in the assembly of N *indistinguishable* particles, $V(\mathbf{r}-\mathrm{r}')$ is the interaction between a single pair of particles, and a_i is the annihilation operator of the particle in the single-particle state $\Phi_i(\mathbf{r})$. One should underline that the basis $\{\Phi_i(\mathbf{r})\}$ should be *complete*, but otherwise arbitrary (it does not have to be orthogonal [10]).

The complete set of $\{\Phi_i(\mathbf{r})\}$ in (2) is in practical calculations not infinite, so we have to resort to a finite subset of $[\Phi_i(\mathbf{r})]$ when performing explicit computations, i.e. constructing *many-particle models*. In this manner, we make the basis *incomplete* in the quantum mechanical sense, even though the model may be well justified on physical grounds as it may contain principal dynamic processes involved. In the first step, we diagonalize H in the Fock space for given trial basis $[\Phi_i(\mathbf{r})]$. Then, as a next step, one can optimize the finite (*incomplete*) subset taken by e.g. minimizing the ground-state energy $E_\mathrm{G} \equiv \langle\Phi_0|\hat{H}|\Phi_0\rangle$ (where $|\Phi_0\rangle$ is the ground-state wavefunction in the Fock-space representation), with respect to the selected subset $[\Phi_i(\mathbf{r})]$. Such a procedure is highly nontrivial, since the determination of $E_\mathrm{G} = E_\mathrm{G}\{\Phi_i(\mathbf{r}), \nabla\Phi_i(\mathbf{r})\}$ requires first the diagonalization of the parametrized Hamiltonian (1) in the Fock space[1] (with the microscopic parameters containing both $[\Phi_i(\mathbf{r})]$ and $[\nabla\Phi_i(\mathbf{r})]$) and, only

[1] One could obtain a complete solution of (1) directly by determining the field operator from the Heisenberg equation of motion for $\hat{\Psi}$ or for the Green function related to it. However, this is usually not feasible if one has to go beyond the Hartree–Fock approximation or the interaction part must be treated nonperturbatively.

after that, setting up an *effective wave equation* for each $\Phi_i(\mathbf{r})$, with E_G treated as a functional of the trial basis $[\Phi_i(\mathbf{r})]$. The resultant renormalized or *self-adjusted wave equation* (SWE) should have a universal meaning to the same degree, as has the starting Hamiltonian (1) in that *incomplete* basis. We call this method of approach EDABI (a combined exact diagonalization–*ab initio* approach). In this manner, only then can the approach to the interacting system be regarded as *completed*, particularly in the situation when the interparticle interaction cannot be regarded as weak, e.g. for *correlated systems*. Obviously, when the correlations are weak, the approach reduces to the Hartree–Fock approximation. This approach has been implemented so far for some exactly soluble models of correlated electrons and for nanochains [11, 12][2] containing up to $N = 16$ atoms used as a trial basis, with adjustable Slater or Gaussian orbitals [4]. Here we present a rather extensive analysis of our method, applicable to both fermion and boson systems, as well as constructing explicitly the multiparticle wavefunction in the simplest atomic situations. The last aspect of the work may be applied to both atomic and molecular systems providing e.g. a systematic approximation scheme in the quantum chemical calculations. In particular, the explicit many-particle wavefunction construction allows for a comparison with the method of the multiconfigurational interaction (MCI) approach [14] utilized in quantum chemistry. Simply put, we develop a relatively straightforward (but not simple!) workable scheme, which is *applicable to both many-electron atoms, molecules and molecular ions, as well as to clusters and nanoscopic systems*.

One can summarize important features of our approach as follows. First, the interaction and the single-particle terms in the many-particle Hamiltonian are treated on an equal footing. Second, the single-particle wavefunction appears in a nonexplicit form in the expression for the microscopic parameters and is determined explicitly from the variational principle for the ground-state energy $E_G = \langle \hat{T} \rangle + \langle \hat{V} \rangle \equiv E_G\{\Phi_i(\mathbf{r})\}$, which leads to the self-adjusted wave equation[3]. Third, the explicit construction of the multiparticle wavefunction $\Psi(\mathbf{r}_1, \cdots, \mathbf{r}_N)$ in terms of the field operators[4] provides a way of systematizing the approximation schemes. Fourth, one does not count twice the interaction, which should be taken with care in e.g. in the LDA + U method. All of these features are particularly important for the systems for which the interaction cannot be treated as a perturbation. Among such systems are cluster and various correlated Fermi and Bose systems, particularly of low dimensionality. Probably the most important formal feature of the present approach is that that by reversing the order of solving the problem (treating first the interaction in the Fock space and only then determining the single-particle wavefunction in the Hilbert space), we *complete* the treatment of strongly correlated systems. Unfortunately, our approach is executable so far only in a limited number of situations. As a side result we also obtain the values of *microscopic parameters* for the parametrized models[5]. In effect, the physical properties can be analysed as a function of interatomic distance, not only as a function of model parameters, and thus provide us with the global minimum for system at hand and for given interatomic distance.

The *self-adjusted wave equation* (SWE), as we shall see, is of nonlocal and nonlinear nature. Hence, it is very difficult to solve it directly. Nonetheless, the main purpose of the

[2] The method presented evolved from an approximate treatment of an extended (one-band) system of correlated electrons discussed by Spałek and Wójcik [13]. This method has also been applied to correlated systems selecting the basis of a single Gaussian instead; see Acquarone *et al* [13]; cf also Fortunelli and Painelli [13].

[3] The method is essentially the same as the variational principle introduced originally by Schrödinger [15]. The Schrödinger equation is obtained by minimizing the expression for the system energy, $\langle \Psi | H_1 | \Psi \rangle$, under the condition $\langle \Psi | \Psi \rangle = 1$. Here, our functional $E_G\{\Phi_i(\mathbf{r})\}$ is much more complicated due to the many-particle nature of the system.

[4] For a lucid introduction to the relation between Fock and Hilbert-space representations of multiparticle states see e.g. [16]; cf also [9]

[5] The parametrized models play a prominent role in the theory of correlated fermionic and bosonic systems, for which exact solutions are avaible in some cases, cf [17]

present paper is to present the solution in the closed variational form and illustrate its character in simple situations, ranging from the atomic physics to nanophysics.

2.2. Renormalized (self-adjusted) wave equation (SWE)

We start with Hamiltonian (1) and write it down in the explicit-spin basis, in which the spin is regarded as an additional coordinate, i.e. in the form

$$\hat{H} = \sum_{\sigma} \int \mathrm{d}^3\mathbf{r}\hat{\Psi}^{\dagger}_{\sigma}(\mathbf{r})H_1(\mathbf{r})\hat{\Psi}_{\sigma}(\mathbf{r}) + \tfrac{1}{2}\sum_{\sigma_1\sigma_2}\int\int \mathrm{d}^3\mathbf{r}_1\mathrm{d}^3\mathbf{r}_2\hat{\Psi}^{\dagger}_{\sigma_1}(\mathbf{r}_1)\hat{\Psi}^{\dagger}_{\sigma_2}(\mathbf{r}_2)V(\mathbf{r}_1-\mathbf{r}_2)\hat{\Psi}_{\sigma_2}(\mathbf{r}_2)\hat{\Psi}_{\sigma_1}(\mathbf{r}_1). \tag{3}$$

We define the spin-dependent field operator as

$$\hat{\Psi}_{\sigma}(\mathbf{r}) = \sum_{i=1}^{M} w_i(\mathbf{r})\chi_{\sigma}a_{i\sigma}, \tag{4}$$

where $\{w_i(\mathbf{r})\}$ is a *complete* single-particle basis with the set of quantum numbers denoted by i. Note that we regard the Hamiltonians $H_1(\mathbf{r})$ and $V(\mathbf{r}_1-\mathbf{r}_2)$ as spin independent (it is straightforward to generalize the formalism to the case with spin-dependent Hamiltonian, i.e. when magnetic field or spin–orbit interaction are included). Substituting (4) into (3) we obtain the usual form of the Hamiltonian

$$H = \sum_{ij\sigma} t_{ij}a^{\dagger}_{i\sigma}a_{j\sigma} + \tfrac{1}{2}\sum_{ijkl\sigma_1\sigma_2} V_{ijkl}a^{\dagger}_{i\sigma_1}a^{\dagger}_{j\sigma_2}a_{l\sigma_2}a_{k\sigma_1}, \tag{5}$$

with the microscopic parameters defined by

$$t_{ij} \equiv \langle w_i|H_1|w_j\rangle \equiv \int \mathrm{d}^3\mathbf{r}w^{\star}_i(\mathbf{r})H_1(\mathbf{r})w_j(\mathbf{r}), \tag{6}$$

and

$$V_{ijkl} \equiv \langle w_iw_j|V|w_kw_l\rangle \equiv \int \mathrm{d}^3\mathbf{r}_1\mathrm{d}^2\mathrm{d}^3\mathbf{r}_2w^{\star}_i(\mathbf{r}_1)w^{\star}_j(\mathbf{r}_2)V(\mathbf{r}_1-\mathbf{r}_2)w_k(\mathbf{r}_1)w_l(\mathbf{r}_2). \tag{7}$$

In the standard form (5) of the many-particle Hamiltonian the single-and many-particle aspects of the problem are separated in the sense that the calculation of the hopping parameters t_{ij} and their corresponding interactions V_{ijkl}, both containing the single-particle wavefunctions $\{w_i(\mathbf{r})\}$, is separated from the diagonalization procedure of the Hamiltonian in the Fock space[6]. The latter procedure is dependent only on the nature of the commutation relation between the annihilation ($a_{i\sigma}$) and creation ($a^{\dagger}_{j\sigma}$) operators. Thus this two-step procedure can be seen explicitly when we calculate the system ground-state energy

$$E_{\mathrm{G}} \equiv \langle H\rangle = \sum_{ij\sigma} t_{ij}\langle a^{\dagger}_{i\sigma}a_{j\sigma}\rangle + \tfrac{1}{2}\sum_{ijkl\sigma_1\sigma_2} V_{ijkl}\langle a^{\dagger}_{i\sigma_1}a^{\dagger}_{j\sigma_2}a_{l\sigma_2}a_{k\sigma_1}\rangle, \tag{8}$$

where the averaging $\langle\cdots\rangle$ takes place over all accessible occupancies of given single-particle states $|i\sigma_1\rangle$, $|j\sigma_2\rangle$, $|k\sigma_1\rangle$, and $|l\sigma_2\rangle$. Obviously, if we want to consider all occupancies (a grand canonical ensemble), we diagonalize $H-\mu N$, where N is the total number of particles, and only *a posteriori* impose the conditions that $N = \sum_{i\sigma}\langle n_{i\sigma}\rangle$, with $n_{i\sigma} \equiv a^{\dagger}_{i\sigma}a_{i\sigma}$.

So far, the approach is standard [9, 10]. We have proposed [2, 11–13] to close the solution (i.e. the complete calculation of e.g. E_{G}) with the determination of the single-particle basis

[6] Note that the parameters t_{ij} and V_{ijkl} contain the functions $\{w_i(\mathbf{r})\}$ under the integral expressions (6) and (7), so E_{G} is indeed a functional of $\{w_i(\mathbf{r})\}$ and $\{\nabla w_i(\mathbf{r})\}$.

$\{w_i(\mathbf{r})\}$ by treating the expression (8) as a functional of the set of functions $\{w_i(\mathbf{r})\}$ and their gradients. In such a situation the renormalized (self-adjusted) wave equation is determined from the Euler equation for the functional

$$E\{w_i(\mathbf{r})\} \equiv E_{\mathrm{G}}\{w_i(\mathbf{r})\} - \mu N - \sum_{i \geqslant j} \lambda_{ij} \left(\int \mathrm{d}^3\mathbf{r} w_i^\star(\mathbf{r}) w_j(\mathbf{r}) - \delta_{ij} \right), \tag{9}$$

where

$$N = \sum_\sigma \int \mathrm{d}^3(\mathbf{r}) \langle \hat{\Psi}_\sigma^\dagger(\mathbf{r}) \hat{\Psi}_\sigma(\mathbf{r}) \rangle = \sum_{ij\sigma} \int \mathrm{d}^3\mathbf{r} w_i^\star(\mathbf{r}) w_j(\mathbf{r}) \langle a_{i\sigma}^\dagger a_{j\sigma} \rangle,$$

N is the number of particles in the system, and λ_{ij} are the Lagrange multipliers, when the single-particle basis is nonorthonormal.

The general form of this equation in the stationary case and in the grand canonical-ensemble formalism is

$$\frac{\delta(E_{\mathrm{G}} - \mu N)}{\delta w_i^\star(\mathbf{r})} - \nabla \frac{\delta(E_{\mathrm{G}} - \mu N)}{\delta(\nabla w_i^\star(\mathbf{r}))} - \sum_{i \geqslant j} \lambda_{ij} w_j(\mathbf{r}) = 0. \tag{10}$$

We will make a *fundamental* postulate concerning this equation: *as this equation does not contain explicitly the (anti)commutation relations between the creation and annihilation operators, it is equally valid for both fermions and bosons and determines a rigorous, within the class of states included in the definition of* $\hat{\Psi}(\mathbf{r})$, *wave equation for a single-particle wavefunction in the ground state, in the milieu of the remaining* $(N-1)$ *particles*. Additionally, as is implicit in the treatment above, we have defined one global spin-quantization axis for all single-particle states used to define $\hat{\Psi}_\sigma(\mathbf{r})$. In some spin noncollinear systems this is insufficient and will require a more refined treatment. Also, if we use the particle conserving approach to calculate E_{G}, then we put $\mu \equiv 0$ in (10). Likewise, for the orthonormal basis $\{w_i(\mathbf{r})\}$ used to define $\hat{\Psi}_\sigma(\mathbf{r})$ in (4), one puts $\lambda_{ij} \equiv 0$. In the latter case the system (10) represents a set of Euler equations for renormalized Wannier functions. In what follows we discuss examples of application of this equation to fermion systems (it can be applied to Bose systems in the same manner). But first, we define the renormalized many-particle wavefunction as complementing the above renormalized single-particle states $\{w_i(\mathbf{r})\}$ and then discuss the differences with the MCI approach.

2.3. Multiparticle wavefunction from the second-quantization approach

The general N-particle state $|\Phi_N\rangle$ in the Fock space can be defined through the corresponding N-particle wavefunction $\Psi_\alpha(\mathbf{r}_1, \ldots, \mathbf{r}_{\mathbf{N}})$ in the Hilbert space in the following manner [16][7]:

$$|\Phi_N\rangle = \frac{1}{\sqrt{N!}} \int \mathrm{d}^3\mathbf{r}_1 \ldots \mathbf{r}_{\mathbf{N}} \Psi_N(\mathbf{r}_1, \ldots, \mathbf{r}_{\mathbf{N}}) \hat{\Psi}^\dagger(\mathbf{r}_1) \ldots \hat{\Psi}^\dagger(\mathbf{r}_{\mathbf{N}}) |0\rangle, \tag{11}$$

where $|0\rangle$ is the vacuum state. One can reverse this relation and a simple algebra yields the following expression for the wavefunction $\Psi_\alpha(\mathbf{r}_1, \ldots, \mathbf{r}_{\mathbf{N}})$ in terms of $|\Phi_N\rangle$:

$$\Psi_\alpha(\mathbf{r}_1, \ldots, \mathbf{r}_{\mathbf{N}}) = \frac{1}{\sqrt{N!}} \langle 0 | \hat{\Psi}(\mathbf{r}_1) \ldots \hat{\Psi}(\mathbf{r}_{\mathbf{N}}) | \Phi_N \rangle. \tag{12}$$

In other words, to obtain the wavefunction in the coordinate representation, we not only annihilate N particles from the state $|\Phi_N\rangle$, but also project out the thus obtained result onto the Fock vacuum state and normalize it by the factor $(N!)^{-1/2}$. Usually, the formula (12) is

[7] The relativistic and nonrelativistic field quantizations for an arbitrary single-particle basis were compared first in [9].

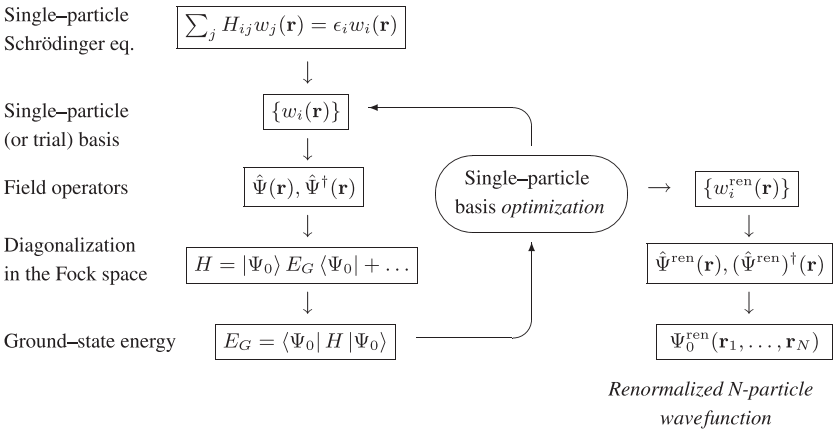

Figure 1. Flow-chart describing the scheme of the EDABI method. For details see the main text. When selecting the Gaussian starting single-particle set, the topmost block should be disregarded.

not used as we proceed from first to second quantization. Now, *the crucial point* is based on the observation that if we substitute in the field operator $\hat{\Psi}(\mathbf{r})$ the renormalized wavefunctions obtained from equation (10), then we should obtain the renormalized field operator and, as a consequence, the renormalized multiparticle wavefunction $\Psi_\alpha(\mathbf{r}_1, \ldots, \mathbf{r_N})$ from relation (12). This last step of inserting the renormalized field operator completes the procedure of a formal treatment of the many-particle system, which avoids writing down explicitly the N-particle Schrödinger equation. The whole approach is schematically represented in figure 1. This scheme provides an exact renormalized single-particle wavefunction from equation (10) and the exact N-particle wavefunction provided we can diagonalize the second-quantized model Hamiltonian (5) for the problem at hand. We shall see next that we can also approach the true solution step by step.

2.4. Finite-basis approximation for the field operator: difference with the multiconfiguration interaction (MCI) approach

The field operator $\hat{\Psi}(\mathbf{r})$ defined in terms of the sum over a complete basis $\{w_i(\mathbf{r})\}$ contains an infinite number of single-particle states. We assume that, in general, we represent the field operator by M wavefunctions $\{w_i(\mathbf{r})\}$. Explicitly,

$$\hat{\Psi}(\mathbf{r}) \equiv \sum_{i=1}^{\infty} w_i(\mathbf{r}) a_i \simeq \sum_{i=1}^{M} w_i(\mathbf{r}) a_i, \tag{13}$$

with i representing a complete set of quantum numbers and M being a finite number. This approximation represents one of the most *fundamental* features of constructing theoretical models. The neglected states usually represent highly excited (and thus negligible) states of the system. We can then write the approximate N-particle wavefunction ($N \leqslant M$) in the following manner:

$$\Psi_\alpha(\mathbf{r}_1, \ldots, \mathbf{r_n}) = \frac{1}{\sqrt{N!}} \sum_{i_1, \ldots, i_N = 1}^{M} \langle 0 | a_{i_N} \ldots a_{i_1} | \Phi_N \rangle w_{i_1}(\mathbf{r}_1) \ldots w_{i_N}(\mathbf{r_N}). \tag{14}$$

Recognizing that within the occupation-number space spanned on the states $\{|i_k\rangle\}_{k=1\ldots M}$ we

have the N-particle state in the Fock space of the form

$$|\Phi_N\rangle = \frac{1}{\sqrt{N!}} \sum_{j_1,\ldots,j_N=1}^{M} C_{j_1\ldots j_N} a_{j_1}^{\dagger} \ldots a_{j_N}^{\dagger} |0\rangle, \tag{15}$$

where $C_{j_1\ldots j_N}$ represents the coefficients of the expansion to be determined from a diagonalization procedure. Substituting (15) into (14) we obtain

$$\Psi_\alpha(\mathbf{r}_1, \ldots, \mathbf{r_N}) = \frac{1}{N!} \sum_{i_1,\ldots,i_N=1}^{M} \sum_{j_1,\ldots,j_N=1}^{M} \langle 0|a_{i_1} \ldots a_{i_N} a_{j_1}^{\dagger} \ldots a_{j_N}^{\dagger}|0\rangle C_{j_1\ldots j_N} w_{i_1}(\mathbf{r}_1) \ldots w_{i_N}(\mathbf{r_N}). \tag{16}$$

The expression provides $N!$ nonzero terms each equal to $(-1)^P$, where P represents the sign of the permutation of quantum numbers $(j_1 \ldots j_N)$ with respect to a selected collection $(i_1 \ldots i_N)$. In other words, we can write that

$$\Psi_\alpha(\mathbf{r}_1, \ldots, \mathrm{r_N}) = \frac{1}{N!} \sum_{i_1,\ldots,i_N=1}^{M} C_{i_1\ldots i_N}(A, S)[w_{i_1}(\mathbf{r}_1) \ldots w_{i_N}(\mathbf{r_N})]. \tag{17}$$

We have the same expansion coefficients for both the wavefunction in the Fock space $|\Phi_N\rangle$ and that in the Hilbert space $\Psi_\alpha(\mathbf{r}_1, \ldots, \mathbf{r_N})$! Therefore, the above expression represents the multiconfigurational-interaction wavefunction of N particles distributed among M states with the corresponding weights $C_{i_1\ldots i_N}$ for each configuration, and (A, S) represents respectively the antisymmetrization (Slater determinant) or the symmetrization (simple product $w_{i_1}(\mathbf{r}_1) \ldots w_{i_N}(\mathbf{r_N})$) for the fermions and bosons, respectively. Whereas the MCI used in quantum chemistry [18] is based on variational optimizations of both the coefficients $C_{i_1\ldots i_N}$ and the basis $\{w_i(\mathbf{r})\}$, here the coefficients C are determined from diagonalization in the Fock space, spanned on M states in the Hilbert space and determined from (10). The presence of SWE (10) thus supplements the usual MCI approach.

Summarizing, the differences between the EDABI and the MCI methods, both of which belong to the class of multi-determinant expansion of the N-particle wavefunction, are threefold.

(i) *Historical.* MCI evolved from variational methods of quantum physics and chemistry to include the electronic correlations and hence to obtain a lower value of E_G by starting from a many-particle Schrödinger equation. EDABI represents a procedure of calculating the single-particle wavefunction starting from parametrized models of strongly correlated electrons.

(ii) *Technical.* In MCI, we optimize simultaneously the coefficient expressing the weights of different determinants (representing different micro-configurations), as well as the parameters of the trial single-particle basis. In EDABI, we diagonalize the Hamiltonian expressed in the Fock space (with the help of either analytic or numerical methods), combined with a simultaneous optimization of the orbital size in the resultant ground state.

(iii) *Essential.* In the case of analytically soluble models, EDABI leads formally to the explicit form of the renormalized wave equation, which represents a *nonlinear Schrödinger equation of nonlocal type*. This circumstance opens up a new direction of studies in *mathematical quantum physics*. Additionally, it allows for a direct determination of dynamical correlation functions, transport properties, etc. in the convenient, second-quantization, language.

2.5. An interpretation of the approach: rationale behind the self-adjusted wavefunction in the many-body system

Usually, the choice of starting single-particle basis $\{w_i(\mathbf{r})\}$ is dictated by the physics of the system at hand. Since the creation and annihilation processes are characterized only by the quantum numbers i of these starting single-particle states, one can say that they represent a *particle language* characterizing transitions between these states. The ground-state energy obtained from the diagonalization in the Fock space defines resultant single-particle states, which can be called the *self-adjusted* states, after the optimization of the single-particle wavefunction has been carried out via solving the *self-adjusted wave equation* (SWE)[8,9] or its variational version. In other words, we allow the initial particle wavefunction $w_i(\mathbf{r})$ to *adjust* to the correlated state. In such a scheme the particle and the wave aspects of the single-particle states are intertwined formally, illustrating among other things the particle–wave complementarity, this time in a formal manner. For example, the Born probability density of finding a particle is taken here as $\sum_\sigma \langle \hat{\Psi}^\dagger_\sigma(\mathbf{r})\hat{\Psi}_\sigma(\mathbf{r})\rangle/N$. In what follows we essentially illustrate the method on concrete examples and apply it to nano-systems.

One may ask *the basic question*: why do we reverse the usual sequence of solving the single-particle wave equation first, and only then constructing the field operators in the second-quantization Hamiltonian (or Lagrangian), by solving the many-particle Hamiltonian first and only then readjusting the orbitals? The reason for this is as follows. As said above, in many cases (e.g. for correlated and/or low-dimensional fermionic systems) we encounter the situation when the interaction cannot be regarded as a perturbation and therefore should be treated *at least* on equal footing with the single-particle aspect of the problem. This is because, in general, the interaction may change the class of the stationary-state wavefunction. Such a situation is beautifully illustrated in the example of the metal–insulator phase transition of the Mott–Hubbard type, at which the metallic state represented by the Bloch-type wavefunctions switches to the localized (Wannier-type) states even though those representations are regarded as equivalent from a single-particle point of view. In other words, the interaction determines the particle wavefunction. Furthermore, the electron as a separate entity (lepton) is preserved even in the highly correlated milieu of other particles and, therefore, constructing the self-consistent wave equation (SWE) has a sense as it provides its wavefunction adjusted to the environment.

2.6. Single-particle basis selection and the particle-density space profiles

As we have already mentioned, the selected single-particle basis $w_i(\mathbf{r}) \equiv \{\Phi_i(\mathbf{r})\}$ is determined from the variational principle for $E_G\{\Phi_i(\mathbf{r}), \nabla\Phi_i(\mathbf{r})\}$, and it should satisfy *the self-adjusted wave equation*. Here we solve this equation variationally and take a trial basis $\{\Phi_i(\alpha; \mathbf{r})\}$ dependent on a finite number of parameters $\alpha \equiv \{\alpha_p\}_{p=1,\ldots,K}$. Moreover, if the basis is orthonormal, then the equation can be simplified to the form

$$\frac{\delta(E_G - \mu N)}{\delta\alpha} = 0. \tag{18}$$

[8] The notion of the *self-adjusted state* differs from the concept of *quasiparticle* state invoked by Landau in his theory of Fermi liquids. The Landau quasiparticle results from an *adiabatic* switching of the interaction and therefore the quasiparticle states are in one-to-one correspondence with the states of an ideal quantum gas forming the liquid. Here, the *self-adjusted states* can be either localized or itinerant, as the interparticle interaction cannot be treated perturbationally. The statistical distribution of correlated states can differ from the Fermi–Dirac distribution (cf [8]), as quasimomentum may not be a good quantum number.

[9] In the context of the orbit-size relaxation one can talk about wavefunction renormalization. The statistical distribution is determined by dynamics in the Fock space.

In most applications we select adjustable atomic orbitals as the basic functions $\{\Phi_i(\alpha;\mathbf{r})\}$, which need to be orthonormalized with a special kind of orthonormalization procedure. Additionally, if the number of particles N is conserved by the Hamiltonian H then the term μN in (18) is absent, and the equation reduces to the ordinary energy minimization $E_{\mathrm{G}} \equiv \langle H\rangle$ with respect to the variation parameters $\{\alpha_p\}$.

2.7. A remainder: Wannier basis for an extended periodic system

Let us consider the multi-particle systems for a single-band case for atoms located at positions $\{\mathbf{R}_i\}$ and the basic wavefunctions $\{\Phi_i(\alpha;\mathbf{r})\}$ of the form $\{\Phi(\alpha;\mathbf{r}-\mathbf{R}_i)\}$. The orthonormalization procedure for periodic structures can be obtained by starting with the expression for the *Bloch* function

$$\Phi_{\mathbf{q}}(\alpha;\mathbf{r}) = N_{\mathbf{q}} \sum_{j=1}^{N} \mathrm{e}^{\mathrm{i}\mathbf{q}\cdot\mathbf{R}_j}\Phi_j(\alpha;\mathbf{r}), \tag{19}$$

where $N_{\mathbf{q}}$ is a normalization coefficient. The normalization condition then takes the form

$$\begin{aligned}\langle\Phi_{\mathbf{q}}(\alpha;\mathbf{r})|\Phi_{\mathbf{q}'}(\alpha;\mathbf{r})\rangle &= N^*_{\mathbf{q}}N_{\mathbf{q}'}\sum_{jl}\mathrm{e}^{-\mathrm{i}\mathbf{q}\cdot\mathbf{R}_j+\mathrm{i}\mathbf{q}'\cdot\mathbf{R}_l}\langle\Phi_j(\alpha;\mathbf{r})|\Phi_l(\alpha;\mathbf{r})\rangle \\ &= N^*_{\mathbf{q}}N_{\mathbf{q}'}\sum_{j}\mathrm{e}^{\mathrm{i}(\mathbf{q}'-\mathbf{q})\cdot\mathbf{R}_j}\sum_{l}\mathrm{e}^{\mathrm{i}\mathbf{q}'\cdot(\mathbf{R}_l-\mathbf{R}_j)}S_{lj} \equiv \delta_{\mathbf{q}\mathbf{q}'},\end{aligned} \tag{20}$$

where S_{lj} is an overlap integral. The last sum does not depend on the relative distance, hence

$$\langle\Phi_{\mathbf{q}}(\alpha;\mathbf{r})|\Phi_{\mathbf{q}'}(\alpha;\mathbf{r})\rangle = N^*_{\mathbf{q}}N_{\mathbf{q}'}N\delta_{\mathbf{q}\mathbf{q}'}\sum_{l}\mathrm{e}^{\mathrm{i}\mathbf{q}'\cdot(\mathbf{R}_l-\mathbf{R}_j)}S_{lj} \equiv \delta_{\mathbf{q}\mathbf{q}'}, \tag{21}$$

and thus

$$|N_{\mathbf{q}}| = \left(N\sum_{l}\mathrm{e}^{\mathrm{i}\mathbf{q}\cdot(\mathbf{R}_l-\mathbf{R}_j)}S_{lj}\right)^{-1/2}. \tag{22}$$

As we can see, the above wavefunctions $\{\Phi_{\mathbf{q}}(\alpha;\mathbf{r})\}$ are the *Bloch* functions, from which we can construct the *Wannier* functions $\{w_l(\alpha;\mathbf{r})\}$ in the usual manner, i.e.

$$\begin{aligned}w_l(\alpha;\mathbf{r}) &= \frac{1}{\sqrt{N}}\sum_{\mathbf{q}}\mathrm{e}^{-\mathrm{i}\mathbf{q}\cdot\mathbf{R}_l}\Phi_{\mathbf{q}}(\alpha;\mathbf{r}) = \frac{1}{\sqrt{N}}\sum_{\mathbf{q}}\mathrm{e}^{-\mathrm{i}\mathbf{q}\cdot\mathbf{R}_l}N_{\mathbf{q}}\sum_{j}\mathrm{e}^{\mathrm{i}\mathbf{q}\cdot\mathbf{R}_j}\Phi_j(\alpha;\mathbf{r}) \\ &= \sum_{j}\Phi_j(\alpha;\mathbf{r})\left(\frac{1}{\sqrt{N}}\sum_{\mathbf{q}}N_{\mathbf{q}}\mathrm{e}^{-\mathrm{i}\mathbf{q}\cdot(\mathbf{R}_l-\mathbf{R}_j)}\right) \equiv \sum_{j}\beta_{lj}\Phi_j(\alpha;\mathbf{r}),\end{aligned} \tag{23}$$

where

$$\beta_{lj} = \frac{1}{N}\sum_{\mathbf{q}}\frac{\mathrm{e}^{-\mathrm{i}\mathbf{q}\cdot(\mathbf{R}_l-\mathbf{R}_j)}}{\sqrt{\sum_m \mathrm{e}^{-\mathrm{i}\mathbf{q}\cdot(\mathbf{R}_n-\mathbf{R}_m)}S_{mn}}}. \tag{24}$$

The orthonormal Wannier set $\{w_l(\alpha;\mathbf{r})\}$ obtained with the help of the above procedure is thus a set of linear combinations of the originally nonorthonormal atomic orbitals. Moreover, the coefficients $\{\beta_{lj}\}$ depend only on $\mathbf{R}_l-\mathbf{R}_j$ and satisfy the relation $\beta_{lj} = \beta^*_{jl}$.

2.8. Wannier functions for finite systems

The above procedure can be applied with modifications to finite cluster systems. We start from the decomposition

$$w_l(\alpha;\mathbf{r}) = \sum_{j=1}^{M}\beta_{lj}\Phi_j(\alpha;\mathbf{r}), \tag{25}$$

with the normalization condition in the form

$$\langle w_l(\alpha;\mathbf{r})|w_{l'}(\alpha;\mathbf{r})\rangle = \sum_{jk}\beta^*_{lj}\beta_{l'k}\langle\Phi_j(\alpha;\mathbf{r})|\Phi_k(\alpha;\mathbf{r})\rangle = \sum_{jk}\beta^*_{lj}\beta_{l'k}S_{kj} \equiv \delta_{ll'}. \tag{26}$$

In the matrix language, this condition can be rewritten as

$$\beta S\beta^+ = 1, \tag{27}$$

or, equivalently, as

$$\beta^+\beta = S^{-1}. \tag{28}$$

We choose the β matrix in the form $\beta = \beta^+$; in effect, this choice leads to the relation

$$\beta = S^{-1/2}. \tag{29}$$

The above method is known as the Löwdin method of determining the orthonormal basis, and for the overlap integral matrix becomes unity if elements of the system are separated from each other at large distances. So, the β matrix then can be written down as

$$\beta = 1 + \sum_{n=1}^{\infty}\frac{(-1)^n\triangle^n}{2^n n!}\prod_{k=1}^{n}(2k-1) = 1 + \sum_{n=1}^{\infty}\triangle^n\prod_{k=1}^{n}\left(\frac{1}{2k}-1\right), \tag{30}$$

where $\triangle = S - 1$. However, the above series does not converge in the tight binding approach and it has to be modified to the form

$$\beta = \left(\frac{(1+C)S}{1+C}\right)^{-1/2}, \tag{31}$$

and thus

$$\beta = (1+C)^{-1/2}\left[1 + \sum_{n=1}^{\infty}\triangle_{\mathrm{C}}^n\prod_{k=1}^{n}\left(\frac{1}{2k}-1\right)\right], \tag{32}$$

where $\triangle_{\mathrm{C}} \equiv S/(1+C) - 1$. The parameter C allows us to manipulate convergence of the series, for it appears in the convergence condition

$$\|\triangle_{\mathrm{C}}\| < 1, \tag{33}$$

that needs to be satisfied for any kind of $\|\cdot\|$ metric. Therefore, we choose the metric

$$\|\triangle_{\mathrm{C}}\|_{\infty} \equiv \max_{ij}\left\{\left|\frac{S_{ij}}{1+C} - \delta_{ij}\right|\right\} = \max\left\{\frac{C}{1+C}; \frac{\max_{i\neq j}|S_{ij}|}{1+C}\right\}. \tag{34}$$

As we can see, the metric satisfies the condition when the parameter C is equal to

$$C = \max_{i\neq j}|S_{ij}|. \tag{35}$$

The method we have just shown can be applied to both single-band and to multiple-band systems. The method can also be applied to disordered systems. In what follows we will select as a starting atomic basis $\{\Phi_i(\mathbf{r})\}$ either a Slater or Gaussian (STO-3G) basis when constructing the Wannier function, and subsequently optimize their size in the correlated state.

2.9. Particle density profiles in space

In the previous section we dealt with the N-particle wavefunction $\Psi(\mathbf{r}_1,\ldots,\mathbf{r}_N)$. Here we show how it can be applied to the evaluation of particle density $n(\mathbf{r})$. We start with the usual definition of the probability density for a single particle:

$$\rho(\mathbf{r}_N) = \int \mathrm{d}^3\mathbf{r}_1\ldots\mathbf{r}_{N-1}|\Psi(\mathbf{r}_1,\ldots,\mathbf{r}_N)|^2. \tag{36}$$

We utilize now expression (4) for the wavefunction we obtained in section 2. In effect,

$$|\Psi(\mathbf{r}_1,\ldots,\mathbf{r}_N)|^2 = \frac{1}{N!}\langle\Phi_N|\widehat{\Psi}^+(\mathbf{r}_N)\ldots\widehat{\Psi}^+(\mathbf{r}_1)|0\rangle\langle 0|\widehat{\Psi}(\mathbf{r}_1)\ldots\widehat{\Psi}(\mathbf{r}_N)|\Phi_N\rangle. \tag{37}$$

We have the particle-number conservation and hence we can rewrite (37) as

$$|\Psi(\mathbf{r}_1,\ldots,\mathbf{r}_N)|^2 = \frac{1}{N!}\langle\Phi_N|\widehat{\Psi}^+(\mathbf{r}_N)\ldots\widehat{\Psi}^+(\mathbf{r}_1)\widehat{\Psi}(\mathbf{r}_1)\ldots\widehat{\Psi}(\mathbf{r}_N)|\Phi_N\rangle. \tag{38}$$

This is because we can insert $\sum_N |N\rangle\langle N|$ instead of $|0\rangle\langle 0|$. The expression for the field operator $\widehat{\Psi}(\mathbf{r})$, defined with the help of the orthonormal basis $\{w_i(\mathbf{r})\}$ in (4), leads to the following relation:

$$\widehat{\Psi}^+(\mathbf{r})\widehat{\Psi}(\mathbf{r}) = \sum_{i_1\sigma_1 i_2\sigma_2} w^*_{i_1}(\mathbf{r})\chi^*_{\sigma_1} w_{i_2}(\mathbf{r})\chi_{\sigma_2} a^+_{i_1\sigma_1} a_{i_2\sigma_2}, \tag{39}$$

and thus

$$\widehat{\Psi}^+(\mathbf{r})\widehat{\Psi}(\mathbf{r}) = \sum_{i_1 i_2\sigma} w^*_{i_1}(\mathbf{r}) w_{i_2}(\mathbf{r}) a^+_{i_1\sigma} a_{i_2\sigma}. \tag{40}$$

Therefore, we can apply the above relation to the expression for $\rho(\mathbf{r}_N)$. Namely, by noting that

$$\rho(\mathbf{r}_N) = \int \mathrm{d}^3\mathbf{r}_2\ldots\mathbf{r}_{N-1}\left(\int \mathrm{d}^3\mathbf{r}_1|\Psi(\mathbf{r}_1,\ldots,\mathbf{r}_N)|^2\right), \tag{41}$$

we can obtain the following series of helpful identities:

$$\begin{aligned}
&\int \mathrm{d}^3\mathbf{r}_1|\Psi(\mathbf{r}_1,\ldots,\mathbf{r}_N)|^2 \\
&\quad= \frac{1}{N!}\int \mathrm{d}^3\mathbf{r}_1\langle\Phi_N|\widehat{\Psi}^+(\mathbf{r}_N)\ldots\widehat{\Psi}^+(\mathbf{r}_1)\widehat{\Psi}(\mathbf{r}_1)\ldots\widehat{\Psi}(\mathbf{r}_N)|\Phi_N\rangle \\
&\quad= \frac{1}{N!}\sum_{i_1 i_2\sigma}\left(\int \mathrm{d}^3\mathbf{r}_1 w^*_{i_1}(\mathbf{r}_1) w_{i_2}(\mathbf{r}_1)\right)\langle\Phi_N|\widehat{\Psi}^+(\mathbf{r}_N)\ldots a^+_{i_1\sigma} a_{i_2\sigma}\ldots\widehat{\Psi}(\mathbf{r}_N)|\Phi_N\rangle \\
&\quad= \frac{1}{N!}\langle\Phi_N|\widehat{\Psi}^+(\mathbf{r}_N)\ldots\widehat{\Psi}^+(\mathbf{r}_2)\sum_{i\sigma} n_{i\sigma}\,\widehat{\Psi}(\mathbf{r}_2)\ldots\widehat{\Psi}(\mathbf{r}_N)|\Phi_N\rangle \\
&\quad= \frac{1}{N!}\langle\Phi_N|\widehat{\Psi}^+(\mathbf{r}_N)\ldots\widehat{\Psi}^+(\mathbf{r}_2)\widehat{\Psi}(\mathbf{r}_2)\ldots\widehat{\Psi}(\mathbf{r}_N)|\Phi_N\rangle.
\end{aligned} \tag{42}$$

The expectation value of the particle-number operator $\sum_{i\sigma} n_{i\sigma}$ is equal to unity for the multi-particle state $\hat{\Psi}(\mathbf{r}_2)\ldots\hat{\Psi}(\mathbf{r}_N)|\Phi_N\rangle \sim |\Phi_{N=1}\rangle$. Obviously, the subsequent procedure applied $N-2$ times leads to the net result

$$\rho(\mathbf{r}_N) = \frac{1}{N}\langle\Phi_N|\widehat{\Psi}^+(\mathbf{r}_N)\widehat{\Psi}(\mathbf{r}_N)|\Phi_N\rangle. \tag{43}$$

This result can be understood if we introduce explicitly the particle-density operator

$$\widehat{n}(\mathbf{r}) \equiv \widehat{\Psi}^+(\mathbf{r})\widehat{\Psi}(\mathbf{r}), \tag{44}$$

and thus the particle density is

$$n(\mathbf{r}) \equiv N\rho(\mathbf{r}) = \langle\Phi_N|\widehat{\Psi}^+(\mathbf{r})\widehat{\Psi}(\mathbf{r})|\Phi_N\rangle. \tag{45}$$

Hence, we obtain the explicit expression for the density of particles using equation (4), i.e.

$$n(\mathbf{r}) = \sum_{i_1 i_2\sigma} w^*_{i_1}(\mathbf{r}) w_{i_2}(\mathbf{r})\langle\Phi_N|a^+_{i_1\sigma} a_{i_2\sigma}|\Phi_N\rangle, \tag{46}$$

or, equivalently

$$n(\mathbf{r}) = \sum_i |w_i(\mathbf{r})|^2 \langle n_i \rangle + \sum_{i_1 \neq i_2} w^*_{i_1}(\mathbf{r}) w_{i_2}(\mathbf{r}) \sum_\sigma \langle a^+_{i_1\sigma} a_{i_2\sigma} \rangle, \tag{47}$$

where averages $\langle \ldots \rangle$ are taken with the N-particle ground state $|\Phi_N\rangle$.

The first of two terms represents the contribution of the particle-number operator to the total density of particles and appears in the *Hartree–Fock* approach as the only term. The second term can provide a significant contribution when the average $\langle a^+_{i_1\sigma} a_{i_2\sigma} \rangle$ is of the same magnitude as the first contribution. Explicitly, if the N-particle function has the form of a simple determinant

$$\Psi_{i_1 \ldots i_N}(\mathbf{r}_1, \ldots, \mathbf{r_N}) = \frac{1}{\sqrt{N!}} \begin{vmatrix} w_{i_1}(\mathbf{r}_1) & \ldots & w_{i_N}(\mathbf{r}_1) \\ \vdots & \ddots & \vdots \\ w_{i_1}(\mathbf{r_N}) & \ldots & w_{i_N}(\mathbf{r_N}) \end{vmatrix}, \tag{48}$$

then the occupancies $\langle n_i \rangle \equiv 1$ in (47) and $\langle a^\dagger_{i_1\sigma} a_{i_2\sigma} \rangle \equiv 0$ for $i_1 \neq i_2$. This is not the case when the multi-configurational form (12) of $\Psi(\mathbf{r}_1, \ldots, \mathbf{r_N})$ is taken, as we shall see in the following. In the remaining part of this paper we discuss the results obtained within this method of approach for various nanosystems.

3. Atomic systems and nanoclusters

In this section we start with the simplest examples of lightest atoms and ions to illustrate the specific features of the EDABI method, as well as to provide an elementary example of the renormalized wave equation. In particular, we systematically enrich up the trial basis to build up the Fock space.

3.1. A didactic example: He atom

We start by selecting as $\{w_i(\mathbf{r})\}$ just two 1s-like states for the He atom $\Phi_\sigma(\mathbf{r}) = (\alpha^3/\pi)^{1/2} \exp(-\alpha r)\chi_\sigma$, where α is the effective inverse radius of the states. In other words, the simplest trial field operator is of the form

$$\hat{\Phi}(\mathbf{r}) = \Phi_\uparrow(\mathbf{r}) a_\uparrow + \Phi_\downarrow(\mathbf{r}) a_\downarrow, \tag{49}$$

where a_σ is the annihilation operator of the particle in the state $\Phi_\sigma(\mathbf{r})$. The Hamiltonian in the second quantization for this two-element basis has then the form

$$H = \epsilon_{\mathrm{a}}(n_\uparrow + n_\downarrow) + U n_\uparrow n_\downarrow, \tag{50}$$

where $n_\uparrow = a^\dagger_\uparrow a_\uparrow$, whereas

$$\epsilon_{\mathrm{a}} = \langle \Phi_\sigma | H_1 | \Phi_\sigma \rangle, \tag{51}$$

and

$$U = \langle \Phi_\sigma \Phi_{\overline{\sigma}} | V | \Phi_{\overline{\sigma}} \Phi_\sigma \rangle \tag{52}$$

are the matrix elements of the single-particle part defined as

$$H_1 = -\frac{\hbar^2}{2m}\nabla_1^2 - \frac{\hbar^2}{2m}\nabla_2^2 - \frac{2e^2}{\kappa_0 r_1} - \frac{2e^2}{\kappa_0 r_2} \overset{a.u.}{\equiv} -\nabla_1^2 - \nabla_2^2 - \frac{4}{r_1} - \frac{4}{r_2} \tag{53}$$

and of the Coulomb interaction

$$V = \frac{e^2}{\kappa_0 |\mathbf{r}_1 - \mathbf{r}_2|} \overset{a.u.}{\equiv} \frac{2}{|\mathbf{r}_1 - \mathbf{r}_2|}, \tag{54}$$

with the corresponding definitions in atomic units after the second equality sign. The only eigenvalue of (50) is obtained for the state $a^\dagger_\uparrow a^\dagger_\downarrow|0\rangle$ and is $E = 2\epsilon_a + U$. This total energy is then minimized with respect to α to obtain the well known variational estimate of both α and the ground-state energy E_G, as discussed before [2]. However, we may look at the problem differently. As the approximate field operator can be defined in an arbitrary basis, we may regard the eigenvalue E as a functional of $\Phi_\sigma(\mathbf{r})$, since the functions are under the integral expressions. Therefore, the true wavefunction is obtained from the Euler equation for the functional under the proviso that the wavefunction is normalized. This means that we minimize the functional

$$E\{\Phi_\sigma(\mathbf{r})\} = \sum_\sigma \int \mathrm{d}^3 r\, \Phi^*_\sigma(\mathbf{r}) H_1(\mathbf{r}) \Phi_\sigma(\mathbf{r}) + \tfrac{1}{2} \sum_\sigma \int \mathrm{d}^3 r \mathrm{d}^3 r' |\Phi_\sigma(\mathbf{r})|^2 V_{12}(\mathbf{r}-\mathbf{r}') |\Phi_{\overline{\sigma}}(\mathbf{r})|^2. \tag{55}$$

In effect, the Euler equation take the form of the unrestricted Hartree–Fock equations for $\Phi_\sigma(\mathbf{r})$

$$\left(\nabla^2 - \frac{2e^2}{\kappa_0 r}\right) \Phi_\sigma(\mathbf{r}) + \Phi_\sigma(\mathbf{r}) \int \mathrm{d}^2 r' \frac{e^2}{\kappa_0 |\mathbf{r}-\mathbf{r}'|} |\Phi_{\overline{\sigma}}(\mathbf{r}')|^2 = \lambda \Phi_\sigma(\mathbf{r}). \tag{56}$$

Thus we can see that taking in the simplest case just two spin orbitals we obtain the well known variational estimate [19] for α and E_G for the He atom: $\alpha = 27/(16a_0)$ and $E_G = -5.695$ Ryd, where $a_0 \simeq 0.53$ Å is the 1s Bohr orbit radius.

Obviously, the proposed expression (49) of the field operator is the simplest one, though it leads to nontrivial results even though the trial atomic basis $\{\Phi_\sigma(\mathbf{r})\}$ is far from being complete in the quantum mechanical sense. However, we can improve systematically on the basis by selecting a richer basis than that in (49). The further step in this direction is discussed next.

3.2. The basis enrichment for the lightest atoms and ions: He, Li

We can expand the field operator in the basis involving the higher order irreducible representations of the rotation group with $n = 2$, which in the variational scheme involve including, apart from the $\Psi_{1s}(\mathbf{r})$ orbital, also the higher $\Psi_{2s}(\mathbf{r})$ and $\Psi_{2pm}(\mathbf{r})$, with $m = \pm 1, 0$ (i.e. the next shell); all of them involving the adjustment of the corresponding orbital characteristics α_i, $i = 1s, 2s$ and $2pm$. The field operator is then

$$\hat{\Psi}(\mathbf{r}) = \sum_\sigma \left[w_{1s}(\mathbf{r}) \chi_{1\sigma} a_{1\sigma} + w_{2s}(\mathbf{r}) \chi_{2\sigma} a_{2\sigma} + \sum_{m=-1}^{+1} w_{2pm}(\mathbf{r}) \chi_{m\sigma} a_{2pm\sigma} \right] \equiv \sum_{i\sigma} w_i(\mathbf{r}) \chi_{i\sigma} a_{i\sigma}, \tag{57}$$

where $w_i(\mathbf{r})$ are orthogonalized orbitals obtained from the nonorthogonal atomic[10] basis $\{\Psi_i(\mathbf{r})\}$ in a standard manner. The Fock space spanned on $2 + 2 + 6 = 10$ trial spin orbitals contains $D = \binom{2M}{N_e}$ dimensions, where $M = 5$ now and $N_e = 2, 3$ is the number of electrons for He and Li, respectively. This means that $D = 45$ and 120 in these two cases and we have to diagonalize the Hamiltonian matrices of this size to determine the ground and the lowest excited states. One should note that we construct and subsequently diagonalize the $\langle i|H|j\rangle$ matrix in the Fock space for (fixed) parameters ϵ_a, t_{ij}, and V_{kl}. After the diagonalization has

[10] Note that the atomic orbitals 1s and 2s are not orthogonal to each other for arbitrary values of their spatial extents $1/\alpha_i$. The 2p orbitals are orthogonal to each other and to s orbitals, since they contain a nontrivial angular dependence expressed via spherical harmonics $Y_l^m(\theta, \phi)$.

Table 1. Optimized Bohr-orbit radii $a_i = \alpha_i^{-1}$ of 1s, 2s, and 2p orbits (in units of a_0), the overlap S between renormalized 1s and 2s states, and the ground-state energy for the lightest atoms and ions (five Slater orbitals taken).

	a_{1s}	a_{2s}	a_{2p}	S	E_G (Ryd)
H	1	2	2	0	−1
H^-	0.9696	1.6485	1.017	−0.1	−1.048 7
He	0.4274	0.5731	0.4068	−0.272	−5.794 04
He^-	1.831	1.1416	0.4354	−0.781	−5.100 58
Li	0.3725	1.066	0.2521	0.15	−14.833 4
Be^+	0.2708	0.683	0.1829	0.109	−28.528 6

been carried out, we readjust the wavefunction and start the whole procedure again until the absolute minimum is reached (cf figure 1).

By diagonalizing the corresponding Hamiltonian matrices and subsequently minimizing the lowest eigenvalue with respect to the parameters α_i—the inverse radial extensions of the corresponding wavefunctions, we obtain the results presented in table 1 (the values a_{2pm} are all equal within the numerical accuracy $\sim 10^{-6}$). For example, the ground-state energy of He is $E_G = -5.794$ Ryd, which is close to the accepted 'exact' value [19] −5.8074, given the simplicity of our approach. Further improvement is feasible by either including the $n = 3$ states or by resorting to the Gaussian basis; these are not performed in this part (see the next sections). Instead, we elaborate on two additional features.

First, we can represent the ground-state two-particle spin-singlet wavefunction for the He atom taking $\hat{\Psi}(\mathbf{r}|)$ in the form (57), which has the following form [6]:

$$\begin{aligned}|\Psi_0^{He}\rangle = (&-0.799\,211 a^+_{1s\downarrow}a^+_{1s\uparrow} + 0.411\,751 a^+_{1s\downarrow}a^+_{2s\uparrow} - 0.411\,751 a^+_{1s\uparrow}a^+_{2s\downarrow}\\ &- 0.135\,451 a^+_{2s\downarrow}a^+_{2s\uparrow} + 0.035\,7708 a^+_{2p0\downarrow}a^+_{2p0\uparrow} + 0.035\,7641 a^+_{2p1\downarrow}a^+_{2p-1\uparrow}\\ &- 0.035\,7641 a^+_{2p1\uparrow}a^+_{2p-1\downarrow})|0\rangle, \end{aligned} \tag{58}$$

Similarly, the $S^z = +1/2$ state for the Li atom is of the form

$$\begin{aligned}|\Psi_0^{Li}\rangle = (&0.997\,499 a^+_{1s\downarrow}a^+_{1s\uparrow}a^+_{2s\uparrow} - 0.057\,0249 a^+_{1s\uparrow}a^+_{2s\downarrow}a^+_{2s\uparrow}\\ &+ 0.003\,9591 a^+_{1s\uparrow}a^+_{2p0\downarrow}a^+_{2p0\uparrow} + 0.003\,959\,02 a^+_{1s\uparrow}a^+_{2p1\downarrow}a^+_{2p-1\uparrow}\\ &- 0.003\,958\,94 a^+_{1s\uparrow}a^+_{2p1\uparrow}a^+_{2p-1\downarrow} - 0.023\,783 a^+_{2s\uparrow}a^+_{2p0\downarrow}a^+_{2p0\uparrow}\\ &- 0.023\,7806 a^+_{2s\uparrow}a^+_{2p1\downarrow}a^+_{2p-1\uparrow} + 0.023\,7806 a^+_{2s\uparrow}a^+_{2p1\uparrow}a^+_{2p-1\downarrow})|0\rangle. \end{aligned} \tag{59}$$

We see that the probability of encountering the configuration $1s^2$ in He is less than $2/3$, whereas the corresponding configuration $1s^22s$ for Li almost coincides with that for the hydrogenic-like picture. The reason for the difference is that the overlap integral between 1s and 2s states $S = \langle 1s|2s\rangle$ in the former case is large and the virtual transitions $1s \rightleftharpoons 2s$ do not involve a substantial change in of the Coulomb energy. These wavefunctions can be used to evaluate any ground-state characteristic by calculating $\langle\Psi_G|\hat{O}|\Psi_G\rangle$ for $\hat{O}$ represented in the second quantized form. For example, the atom dipole moment operator is $\hat{\mathbf{d}} = e\int d^3r\,\hat{\Psi}^\dagger(\mathbf{r})\mathbf{x}\hat{\Psi}(\mathbf{r})$, etc.

The second feature is connected with determination of the microscopic parameters V_{ijkl} in our Hamiltonian, since their knowledge is crucial for atomic cluster calculations, as well as the determination of physical properties of extended systems as a function of the lattice parameter. Namely, we can rewrite the Hamiltonian (5) for the case of a single atom within the basis (57)

Table 2. Microscopic parameters (in Ryd) of the selected atoms and ions all quantities are calculated for the orthogonalized atomic states. t is the 1s–2s hopping magnitude, U_i is the intraorbital Coulomb interaction ($i = 1\text{s}(1), 2\text{s}(2), m = 0(3)$, and $m = \pm 1(p)$), whereas K_{ij} and J_{ij} are the interorbital Coulomb and exchange interaction parameters.

	t	U_1	U_2	U_3	U_p	K_{12}	K_{13}	K_{23}	J_{12}	J_{13}	J_{23}
H^-	0.057	1.333	0.369	0.77	0.728	0.519	0.878	0.457	0.061	0.138	0.035
He	1.186	3.278	1.086	1.924	1.821	1.527	2.192	1.289	0.212	0.348	0.115
He^-	−1.1414	1.232	0.764	1.798	1.701	0.929	1.421	1.041	0.269	0.28	0.102
Li	−0.654	3.267	0.533	3.105	2.938	0.749	3.021	0.743	0.06	0.606	0.014
Be^+	−0.929	4.509	0.869	4.279	4.049	1.191	4.168	1.175	0.105	0.837	0.025

in the form

$$H = \sum_{i\sigma} \epsilon_i n_{i\sigma} + t \sum_{\sigma} (a^\dagger_{2\sigma} a_{1\sigma} + a^\dagger_{1\sigma} a_{2\sigma}) + \sum_{i=1}^{5} U_i n_{i\uparrow} n_{i\downarrow} + \tfrac{1}{2} \sum_{i\neq j} K_{ij} n_i n_j$$
$$- \tfrac{1}{2} \sum_{i\neq j} J_{ij} \left(\mathbf{S_i} \cdot \mathbf{S_j} - \tfrac{1}{2} n_i n_j \right) + \sum_{i\neq j} J_{ij} a^\dagger_{i\uparrow} a^\dagger_{i\downarrow} a_{j\downarrow} a_{j\uparrow} + \sum_{i\neq j\sigma} V_{ij} n_{i\bar{\sigma}} a^\dagger_{i\sigma} a_{j\sigma}. \tag{60}$$

t is the hopping integral between 1s and 2s states, U_i are the intraorbital Coulomb interactions, K_{ij} are their interorbital counterparts, V_{ij} is the so-called correlated hopping integral, and J_{ij} is the direct exchange integral, for states i and $j = 1, \ldots, 5$. The principal parameters for the atoms and selected ions are provided in table 2. We can draw the following interpretation from this analysis. The calculated energy difference ΔE for He between the ground-state singlet and the first excited triplet is $-2.3707 - (-5.794) \simeq 3.423$ Ryd (the singlet $1\text{s} \uparrow 2\text{s} \downarrow$ is still 1 Ryd higher). The corresponding energy of the Coulomb interaction in the 1s^2 configuration is $U_1 = 3.278$, a value comparable to ΔE. Additionally, the Coulomb interaction in the $1\text{s} \uparrow 2\text{s} \downarrow$ state is ≈1.5 Ryd, a substantially lower value. The relative energetics tells us why we have a substantial admixture of the excited $1\text{s} \uparrow 2\text{s} \downarrow$ state to the singlet 1s^2. In other words, a substantial Coulomb interaction ruins the hydrogenic-like scheme, although the actual values could still be improved by further enriching the trial basis.

One may ask how the renormalized wave equation would look in the present situation. The answer to this question is already not brief for the basis containing $M = 5$ starting states $\{w_i(\mathbf{r})\}$; we return to this question in a slightly simpler case of molecular states, which we consider next.

3.3. H_2 molecule and the H_2^- and H_2^+ ions

In this subsection we consider the H_2 and Li_2 molecules, and the H_2^- ion molecule. For the illustration of the method we have plotted in figure 2 the level scheme for the H_2 and H_2^- systems. We consider first the situation with only one 1s-like orbital per atom. For H_2 we have $\binom{4}{2} = 6$ two-particle states [2]. For this purpose, we start with the parametrized Hamiltonian (60), where subscripts 'i' and 'j' label now the two atomic sites and hence $U_1 = U_2 = U$, $K_{12} = K$, $J_{12} = J$, $V_{12} = V$, and $\epsilon_1 = \epsilon_2 = \epsilon_a$. The lowest eigenstate for H_2 is

$$E_G \equiv \lambda_5 = 2\epsilon_a + \tfrac{1}{2}(U + K) + J - \tfrac{1}{2}\left[(U - K)^2 + 16(t + V)^2\right]^{1/2}, \tag{61}$$

and the corresponding singlet ground state in the Fock space has the form

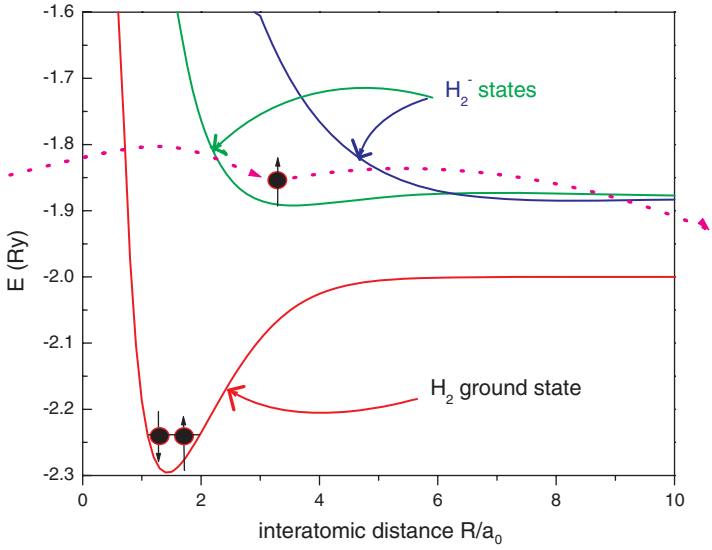

Figure 2. The level scheme of the H_2 ground state and the lowest H_2^- states as a function of the interatomic distance R. The hopping electron illustrates the relevance of the H_2^- ionic configuration when measuring the tunnelling conductivity of the H_2 system.

$$|G\rangle = \frac{1}{\sqrt{2D(D-U+K)}} \times \left\{ \frac{4(t+V)}{\sqrt{2}}(a^\dagger_{1\uparrow}a^\dagger_{2\downarrow} - a^\dagger_{1\downarrow}a^\dagger_{2\uparrow}) - \frac{(D-U+K)}{\sqrt{2}}(a^\dagger_{1\uparrow}a^\dagger_{2\downarrow} + a^\dagger_{1\downarrow}a^\dagger_{2\uparrow}) \right\} |0\rangle, \tag{62}$$

where

$$D \equiv \left[(U-K)^2 + 16(t+V)^2\right]^{1/2}.$$

The lowest spin-singlet eigenstate has an admixture of symmetric ionic state $\frac{1}{\sqrt{2}}(a^\dagger_{1\uparrow}a^\dagger_{2\downarrow} + a^\dagger_{1\downarrow}a^\dagger_{2\uparrow})$. Therefore, to see the difference with either the Hartree–Fock or Heitler–London approach to H_2 we construct the two-particle wavefunction for the ground state according to the prescription

$$\Phi_0(\mathbf{r}_1, \mathbf{r}_2) \equiv \frac{1}{\sqrt{2}}\langle 0|\hat{\Psi}(\mathbf{r}_1)\hat{\Psi}(\mathbf{r}_2)|G\rangle. \tag{63}$$

Taking $\hat{\Psi}(\mathbf{r}) = \sum_{i=1}^{2}\sum_{\sigma=\uparrow}^{\downarrow}\Phi_i(\mathbf{r})\chi_\sigma(\mathbf{r})$, we obtain that

$$\Phi_0(\mathbf{r}_1, \mathbf{r}_2) = \frac{2(t+V)}{\sqrt{2D(D-U+K)}}\Phi_c(\mathbf{r}_1, \mathbf{r}_2) - \frac{1}{2}\sqrt{\frac{D-U+K}{2D}}\Phi_i(\mathbf{r}_1, \mathbf{r}_2), \tag{64}$$

where the covalent part is

$$\Phi_c(\mathbf{r}_1, \mathbf{r}_2) = [w_1(\mathbf{r}_1)w_2(\mathbf{r}_2) + w_1(\mathbf{r}_2)w_2(\mathbf{r}_1)]\left[\chi_\uparrow(\mathbf{r}_1)\chi_\downarrow(\mathbf{r}_2) - \chi_\downarrow(\mathbf{r}_1)\chi_\uparrow(\mathbf{r}_2)\right], \tag{65}$$

whereas the ionic part takes the form

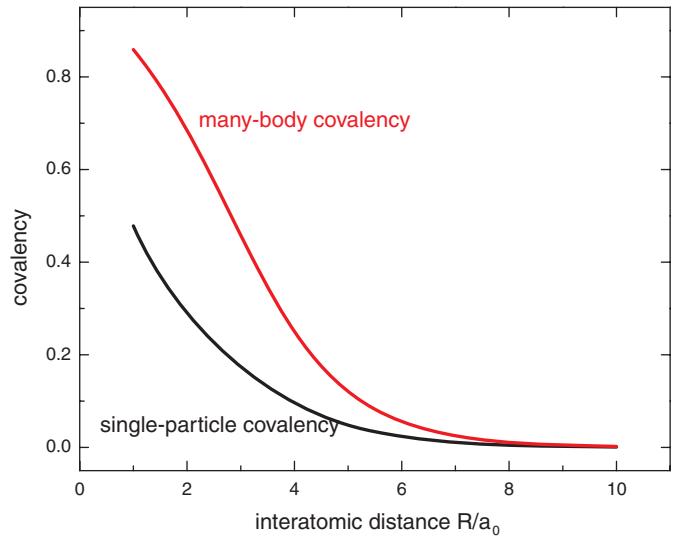

Figure 3. The single-particle (γ) and many-body ($\gamma_{\rm mb}$) covalency factors for the H_2 wavefunctions. For details see the main text.

$$\Phi_i(\mathbf{r}_1, \mathbf{r}_2) = [w_1(\mathbf{r}_1)w_1(\mathbf{r}_2) + w_2(\mathbf{r}_1)w_2(\mathbf{r}_2)]\left[\chi_\uparrow(\mathbf{r}_1)\chi_\downarrow(\mathbf{r}_2) - \chi_\downarrow(\mathbf{r}_1)\chi_\uparrow(\mathbf{r}_2)\right]. \tag{66}$$

The ratio of the coefficients before $\Phi_c(\mathbf{r}_1, \mathbf{r}_2)$ and $\Phi_i(\mathbf{r}_1, \mathbf{r}_2)$ can be regarded as the *many-body covalency* $\gamma_{\rm mb}$. This value should be distinguished from the *single-particle covalency* γ appearing in the definition of the orthogonalized atomic orbital $w_i(\mathbf{r})$:

$$w_i(\mathbf{r}) = \beta\left[\Phi_i(\mathbf{r}) - \gamma\Phi_j(\mathbf{r})\right], \tag{67}$$

with $j \neq i$. The two quantities are drawn in figure 3. The many-body covalency $\gamma_{\rm mb}$ represents a true degree of multiparticle configurational mixing.

In table 3 we list the energies and the values of the microscopic parameters for H_2 system with optimized orbitals, whereas in table 4 the same is provided for the H_2^- molecular ion. One should notice a drastic difference for the so-called *correlated hopping* matrix element V in the two cases. The same holds true for the direct exchange integral J (ferromagnetic). This exchange integral is always decisively smaller than that for the antiferromagnetic kinetic exchange, $J_{\rm kex} = 4(t + V)^2/(U - K)$. The virtual interatomic hopping processes leading to the strong kinetic exchange are the source of the singlet nature of the H_2 ground state. The H_2^- ground state is unstable with respect to the dissociation into H_2 and e^-, in contrast to the H^- case. However, the energetics of such a state is important when calculating e.g. the metallization of molecular hydrogen or determining the tunnelling conductivity through the H_2 molecule, as shown schematically in figure 2. This last Figure illustrates the method of determining the energetics of excited states of H_2 by measuring e.g. the tunnelling conductivity (i.e. via the H_2^- intermediate state; see below).

For the sake of completeness, we have provided in figure 4 the energy levels versus R for H_2, H_2^-, and H_2^+ ions and have labelled both the bonding (B) and antibonding (AB) level positions. We see that the distance between H_2 and H_2^- levels is much smaller than the distance between H_2 and H_2^+ states. This will lead to the asymmetry in the tunnelling conductivity when reversing the bias voltage sign, as discussed in detail in section 5.

Table 3. Ground-state energy and microscopic parameters (in Ryd) for the H_2 molecule. The last column represents the kinetic exchange integral characterizing intersite antiferromagnetic exchange.

R/a	E_G/N	ϵ_a	t	U	K	V (mRyd)	J (mRyd)	$\frac{4(t+V)^2}{U-K}$ (mRyd)
1.0	−1.0937	−1.6555	−1.1719	1.8582	1.1334	−13.5502	26.254 5	7755.52
1.5	−1.1472	−1.7528	−0.6784	1.6265	0.9331	−11.6875	21.252 9	2747.41
2.0	−1.1177	−1.722	−0.4274	1.4747	0.7925	−11.5774	16.921 8	1130.19
2.5	−1.0787	−1.6598	−0.2833	1.3769	0.6887	−12.0544	13.149 8	507.209
3.0	−1.0469	−1.5947	−0.1932	1.3171	0.6077	−12.594	9.815 3	238.939
3.5	−1.0254	−1.5347	−0.1333	1.2835	0.5414	−12.8122	6.922 4	115.143
4.0	−1.0127	−1.4816	−0.0919	1.2663	0.4854	−12.441	4.573 6	55.8193
4.5	−1.006	−1.4355	−0.0629	1.2579	0.4377	−11.4414	2.836 7	26.9722
5.0	−1.0028	−1.3957	−0.0426	1.2539	0.3970	−9.9894	1.665 2	12.9352
5.5	−1.0012	−1.3616	−0.0286	1.2519	0.3623	−8.3378	0.933 4	6.1455
6.0	−1.0005	−1.3324	−0.01905	1.251	0.3327	−6.7029	0.503 3	2.8902
6.5	−1.00024	−1.3073	−0.0126	1.2505	0.3075	−5.2242	0.262 6	1.3452
7.0	−1.0001	−1.2855	−0.0083	1.2503	0.2856	−3.9685	0.133 3	0.6197
7.5	−1.00004	−1.2666	−0.0054	1.2501	0.2666	−2.9509	0.066	0.2826
8.0	−1.00002	−1.25	−0.0035	1.25006	0.25	−2.1551	0.032	0.1277
8.5	−1.00001	−1.2353	−0.0023	1.25003	0.2353	−1.5501	0.015 23	0.0572
9.0	−1.	−1.2222	−0.0015	1.25001	0.2222	−1.1005	0.007 1	0.0254
9.5	−1.	−1.2105	−0.0009	1.25001	0.2105	−0.7725	0.003 3	0.0112
10.0	−1.	−1.2	−0.0006	1.25	0.2	−0.5371	0.001 5	0.0049

Table 4. The same as in table 3 for H_2^- ion.

R/a	E_G/N	ϵ_a	t	U	K	V	J	$\frac{4(t+V)^2}{U-K}$
1.0	−0.4591	−1.6607	−0.5869	1.1414	0.7360	−0.0105	0.016 3	3.522 0
1.5	−0.7659	−1.6647	−0.4285	1.1279	0.6983	−0.0085	0.016 1	1.778 2
2.0	−0.8813	−1.6259	−0.3083	1.0979	0.6474	−0.0078	0.015 0	0.887 1
2.5	−0.9264	−1.5737	−0.2221	1.0692	0.5961	−0.0079	0.013 3	0.447 6
3.0	−0.9423	−1.5204	−0.1603	1.0466	0.5476	−0.0086	0.011 3	0.228 6
3.5	−0.9460	−1.4704	−0.1154	1.0305	0.5025	−0.0093	0.009 1	0.117 9
4.0	−0.9450	−1.4252	−0.0826	1.0196	0.4608	−0.0099	0.007 1	0.061 2
4.5	−0.9426	−1.3848	−0.0585	1.0126	0.4226	−0.0101	0.005 2	0.031 9
5.0	−0.9402	−1.3491	−0.0410	1.0080	0.3881	−0.0099	0.003 7	0.016 7
5.5	−0.9384	−1.3176	−0.0284	1.0051	0.3573	−0.0093	0.002 5	0.008 8
6.0	−0.9373	−1.2901	−0.0194	1.0032	0.3300	−0.0085	0.001 7	0.004 6
6.5	−0.9365	−1.2621	−0.0130	0.9905	0.3058	−0.0075	0.001 1	0.002 5
7.0	−0.9363	−1.2402	−0.0086	0.9876	0.2847	−0.0065	0.000 7	0.001 3
7.5	−0.9365	−1.2211	−0.0056	0.9856	0.2662	−0.0055	0.000 4	0.000 7
8.0	−0.9367	−1.2044	−0.0036	0.9844	0.2498	−0.0046	0.000 3	0.000 4
8.5	−0.9372	−1.1897	−0.0022	0.9839	0.2352	−0.0037	0.000 2	0.000 2
9.0	−0.9376	−1.1768	−0.0013	0.9839	0.2222	−0.0030	0.000 09	0.000 10
9.5	−0.9380	−1.1653	−0.0008	0.9842	0.2105	−0.0024	0.000 05	0.000 05
10.0	−0.9384	−1.1549	−0.0004	0.9848	0.2000	−0.0018	0.000 03	0.000 03

3.4. Hydrogen clusters, H_N

As the next application we consider hydrogen-cluster H_N systems, with $N \leqslant 6$ atoms. We take the atomic-like 1s orbitals $\{\Phi_i(\mathbf{r})\}$ of an adjustable size $a \equiv \alpha^{-1}$, composing the orthogonalized atomic (Wannier) functions $\{w_i(\mathbf{r})\}_{i=1,\ldots,N}$. The cluster of N atoms with N electrons contains

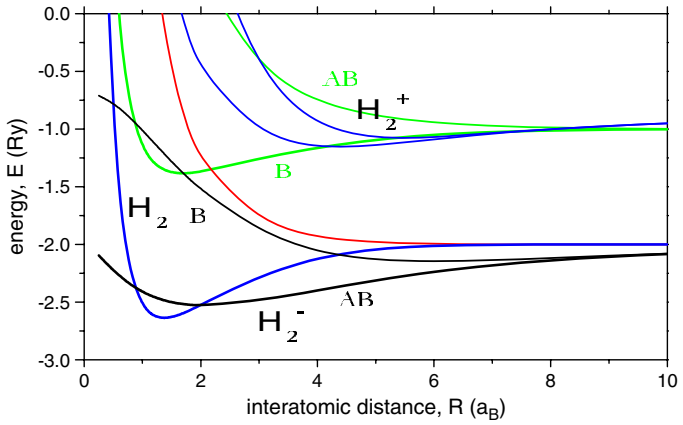

Figure 4. Position of H_2^+ bonding (B) and antibonding (AB) energy levels with respect to those of H_2 and H_2^-, drawn as a function of intermolecular distance.

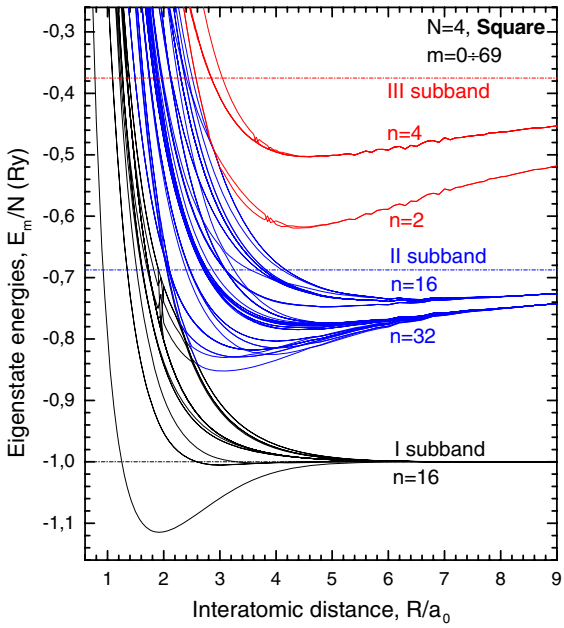

Figure 5. Ground- and excited-state energies for the H_4 square configuration as a function of the interatomic distance.

$\binom{2N}{N}$ states and the second-quantized Hamiltonian is of the form (60), with three- and four-site terms added. The three- and four-site interaction terms are difficult to calculate in the Slater basis (see below). Therefore, we have made an ansatz [7], namely we impose the condition on the trial Wannier function that the three- and four-site matrix elements V_{ijkl} vanish. This allows for an explicit expression of the three- and four-site matrix elements V'_{ijkl} in the atomic representation via the corresponding one- and two-site elements. In figures 5 and 6 we present the results for the ground- and excited-state energies for the square and face-centred-square (fcs) configurations, $N = 4$ and 5, respectively. The states are grouped into manifolds, which

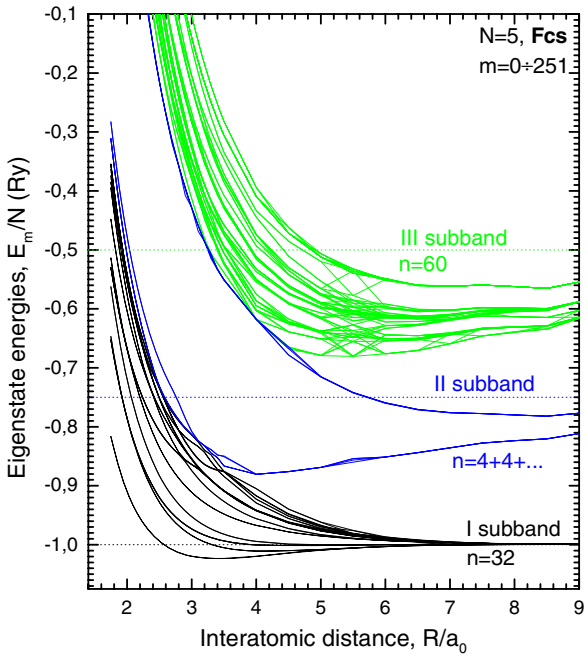

Figure 6. Ground- and excited-state energies for the H_5 face-centred-square (fcs) configuration as a function of the interatomic distance.

are characterized by the number of double occupancies of a single state $w_i(\mathbf{r})$, appearing in the system. The horizontal lines mark the ground state, states with one and two double electron occupancies in the atomic limit (i.e. for large interatomic distance). The manifolds thus correspond to the *Hubbard subbands* introduced for strongly correlated solids [20]. As far as we are aware, our results are the first manifestation of the energy manifold evolution into well separated subbands with the interatomic distance increase. The first two subbands correspond to HOMO and LUMO levels determined in quantum chemical calculation [18]. In figures 7 and 8 we represent the renormalized Wannier function profiles for the face centred square configuration of $N = 5$ atoms, for the central and the corner positions, respectively. Note the small negative values on the nearest-neighbour sites to assure the orthogonality of the functions centred on different sites. Obviously, the atom in the centre of the square is inequivalent to the remaining four corner atoms, as can be see explicitly in figure 9, where the density profile $n(\mathbf{r})$ in the cluster plane, according to formula (47), has been drawn. The electron density near the central atom is decisively smaller, a clear sign of electron-correlation effects induced by the repulsive Coulomb interaction. This assessment is corroborated in figure 10, where the difference from the Hartree–Fock part of the density profile has been presented. These densities should be possible to determine with the help of scanning tunnelling microscopy (STM).

3.5. Energetically stable H_4 clusters and fermionic nanoladders

The H_N clusters of regular-polygon shape are not stable energetically, as the ground state energies in figures 5 and 6 at the minimum (per atom) is above that for the H_2 case. This is because a stable, say, H_4 cluster will reflect strong molecular bonding of each pair of H_2 molecules to saturate the covalent character of the bonding. To prove that this is indeed the

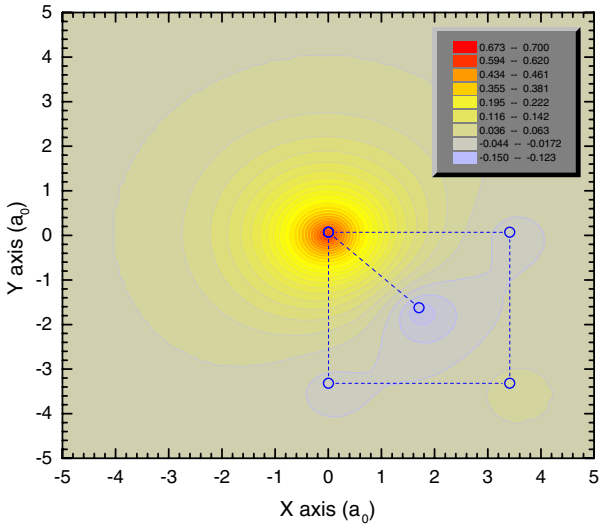

Figure 7. The renormalized Wannier function profile for the central atom in the fcs structure.

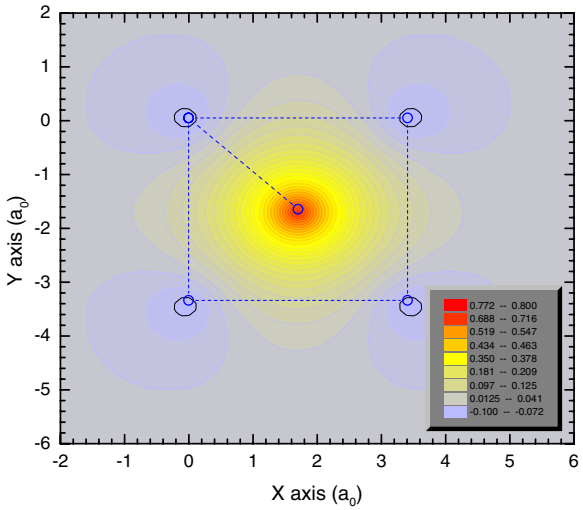

Figure 8. The renormalized Wannier function profile for the corner atom in the fcs structure.

case we have considered an example of a rectangular cluster differentiating between the lateral distance (say, along the bond of the length a) and the horizontal intermolecular distance b. We consider both the planar and the twisted by 90° configurations, as drawn in figure 11. The Gaussian STO-3G basis of an adjustable size α^{-1} has been used in this case, so the three- and four-site interaction terms in the atomic basis are included explicitly. Additionally, the Hamiltonian in the second quantization, only containing the principal one-and two-site interactions, is taken in the form [5]

$$H = \epsilon_{\mathrm{a}}^{\mathrm{eff}} \sum_{i\sigma} n_{i\sigma} + \sum_{i\neq j} t_{ij} a_{i\sigma}^{\dagger} a_{j\sigma} + U \sum_{i} n_{i\uparrow} n_{i\downarrow} + \tfrac{1}{2} \sum_{i\neq j} K_{ij} \delta n_i \delta n_j, \qquad (68)$$

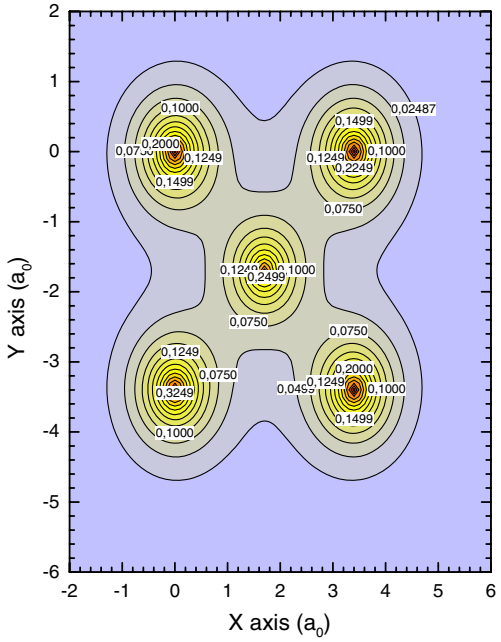

Figure 9. Electron density profile for the H_5 face-centred-square (fcs) structure.

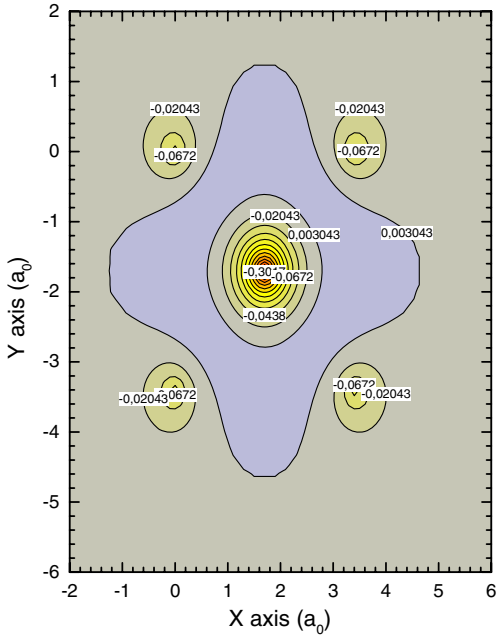

Figure 10. Difference between the calculated density of states and the Hartree–Fock results for the H_5 fcs structure.

where $\delta n_i = 1 - n_i$, $n_i = \sum_\sigma n_{i\sigma}$ and

$$\epsilon_{\mathrm{a}}^{\mathrm{eff}} = \epsilon_{\mathrm{a}} + \frac{1}{2N}\sum_{i\neq j}\left(K_{ij} + \frac{2}{R_{ij}}\right), \tag{69}$$

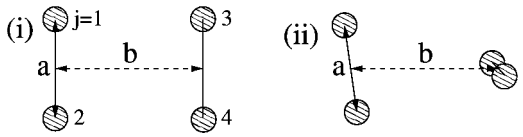

Figure 11. Schematic representation of the H_4 cluster geometries: (i) parallel and (ii) perpendicular orientations of H_2 molecules. Geometrical parameters of the cluster are the bond length a and the intermolecular distance b. The numbering order of the lattice sites j is also provided.

Table 5. The optimal bond length $a_{\min}$, inverse orbital size $\alpha_{\min}$, and the ground-state energy E_G per atom for the planar H_4 cluster (i). The corresponding energy of the molecular dimer $E_G(2H_2)$ is also provided.

b/a_0	$a_{\min}/a_0$	$\alpha_{\min}a_0$	E_G/N	$E_G(2H_2)/N$
1.7	1.3627	1.2231	−0.928 424	−0.922 411
2.0	1.3291	1.2395	−1.019 152	−1.016 365
2.5	1.3518	1.2304	−1.098 551	−1.097 314
3.0	1.3829	1.2157	−1.131 770	−1.131 167
3.5	1.4075	1.2041	−1.144 613	−1.144 317
4.0	1.4238	1.1969	−1.148 598	−1.148 454
5.0	1.4373	1.1911	−1.148 093	−1.148 056
6.0	1.4390	1.1908	−1.145 975	−1.145 964
8.0	1.4375	1.1924	−1.143 651	−1.143 649
10.0	1.4366	1.1929	−1.142 756	−1.142 755
20.0	1.4357	1.1940	−1.141 908	−1.141 908
∞	1.4356	1.1943	−1.141 783	

with the last term in the parenthesis representing the Coulomb repulsion (in atomic units) between the protons placed at the distance R_{ij}, together with the electron–electron intersite repulsion K_{ij} (such a redefinition is necessary to achieve the proper atomic limit, when the nearest-neighbour distance $R \to \infty$). Also, we have to take into account three different hopping integrals: between the nearest neighbours $t_1 = t_{12} = t_{34}$, between the second neighbours $t_2 = t_{13} = t_{24}$, and between the third neighbours $t_3 = t_{14} = t_{23}$. Likewise, we have three intersite Coulomb interactions $\{K_n\}_{n=1,2,3}$.

The basic ground-state characteristics for the two spatial arrangements is provided in tables 5 and 6.

The results are listed as a function of intermolecular distance and include the bond length $a_{\min}$, the inverse Gaussian-function size α, the energy of H_4 and the energy of two H_2 molecules (per atom). The principal feature of these results is that the system is energetically stable against the dissociation into two H_2 molecules (cf the last row in the two situations). The global minima are the following:

(i) for the planar geometry $b_{\min} = 4.32a_0$, $a_{\min} = 1.4303a_0$, $\alpha_{\min} = 1.1937a_0^{-1}$, and $E_G^{\min}/N = -1.149\,061$ Ryd; and
(ii) for the twisted 90° geometry $b_{\min} = 4.13a_0$, $a_{\min} = 1.4318a_0$, $\alpha_{\min} = 1.119\,27a_0^{-1}$, and $E_G^{\min}/N = -1.150\,396$ Ryd.

So, geometry (ii) is the most stable in vacuum and should constitute a building block for the H_2 molecular crystal. Note that we have not included the zero-point motion of the nuclei [2]. The ratio b/a is roughly four, so substantial molecular identity of H_2 pairs survives.

As in all cases before, the knowledge of microscopic parameters is crucial for the larger-cluster or solid-state configurations (Hamiltonian (68) provides the whole dynamics within

Table 6. The optimal bond length $a_{\min}$, inverse orbital size $\alpha_{\min}$, and ground-state energy E_G per atom for the cluster geometry (ii). The corresponding energy of the molecular dimer $E_G(2H_2)$ is also provided.

b/a_0	$a_{\min}/a_0$	$\alpha_{\min}a_0$	E_G/N	$E_G(2H_2)/N$
1.6	1.5796	1.1568	−0.928 235	−0.923 390
2.0	1.3759	1.2206	−1.038 891	−1.037 968
2.5	1.3725	1.2193	−1.108 116	−1.107 803
3.0	1.3947	1.2091	−1.136 931	−1.136 809
3.5	1.4153	1.2000	−1.147 566	−1.147 519
4.0	1.4292	1.1937	−1.150 310	−1.150 293
5.0	1.4397	1.1894	−1.148 674	−1.148 672
6.0	1.4400	1.1897	−1.146 200	−1.146 200
8.0	1.4377	1.1926	−1.143 705	−1.143 705
10.0	1.4367	1.1929	−1.142 774	−1.142 774
20.0	1.4357	1.1940	−1.141 908	−1.141 908
∞	1.4356	1.1943	−1.141 783	

Table 7. Microscopic parameters (in Ryd) for the H_4 cluster configuration (i) calculated in the Gaussian STO-3G basis. Corresponding values of the inverse orbital size $\alpha_{\min}$ and the bond length $a_{\min}$ are provided in table 5.

b/a_0	ϵ_a^{eff}	t_1	t_2	t_3	U	K_1	K_2	K_3
1.7	−0.2354	−0.8610	−0.6622	0.0822	1.811	1.027	0.947	0.728
2.0	−0.3088	−0.8791	−0.5137	0.0617	1.802	1.032	0.872	0.692
2.5	−0.4233	−0.8390	−0.3268	0.0352	1.748	1.007	0.750	0.619
3.0	−0.4925	−0.7983	−0.2067	0.0220	1.702	0.984	0.649	0.553
3.5	−0.5319	−0.7685	−0.1290	0.0150	1.671	0.967	0.567	0.497
4.0	−0.5533	−0.7492	−0.0785	0.0103	1.653	0.957	0.500	0.449
5.0	−0.5689	−0.7316	−0.0267	0.0037	1.639	0.949	0.401	0.373
6.0	−0.5707	−0.7275	−0.0084	0.0007	1.638	0.948	0.334	0.318
8.0	−0.5692	−0.7269	−0.0006	−0.0000	1.640	0.949	0.250	0.243
10.0	−0.5684	−0.7268	−0.0000	−0.0000	1.641	0.950	0.200	0.197
20.0	−0.5673	−0.7272	−0.0000	−0.0000	1.642	0.951	0.100	0.100
∞	−0.5671	−0.7273	0	0	1.642	0.951	0	0

the subspace with one orbital per atom). Therefore, in 7 and 8 we list them for the two configurations considered, as a function of intermolecular distance b (the last row represents the corresponding values for H_2 in the ground state).

The stability of the H_4 cluster raises a very interesting question of stability of H_{2N} ladders, which can be regarded as the simplest fermionic ladders with the frustration of electron spins in the twisted configuration.

For this purpose we have considered planar (i) and 90° twisted (ii) ladders composed of eight to 12 atoms. In figure 12 we display the ground-state energy (per atom) for the nanoladder containing $N = 10$ atoms with periodic boundary conditions. The insets provide the values of the optimal bond length $a_{\min}$ (left) and the inverse atomic (Gaussian) orbital size $\alpha_{\min}$ (right). The Gaussian orbitals (STO-3G basis) have been used to define the single-particle basis. The horizontal dashed line marks the H_2 ground-state energy. One should also note that due to the closed-shell molecular-crystal configuration ($b/a \sim 4$) of the ground state the data almost do not depend on the system size (e.g. analogical results for $N = 8$ fit onto those shown in figure 12 up to the pixel size). The characteristics of the global minima are the following:

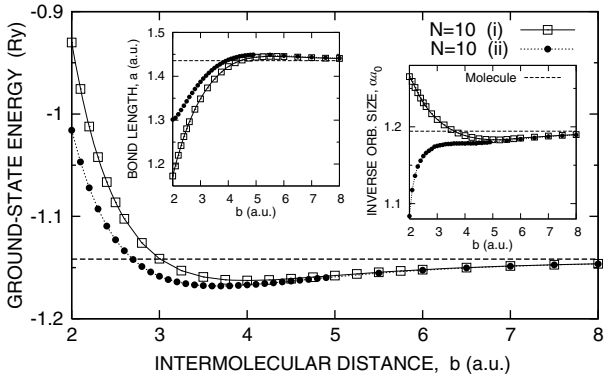

Figure 12. Ground-state energy per atom for the planar ladder of $N = 12$ atoms (a) with a fixed intermolecular distance b (specified in the units of Bohr radius a_0), and (b) the corresponding values of the optimal inverse orbital size $\alpha_{\min}$. Periodic boundary conditions are used. The results for the atomic chain (*dashed* lines) with a lattice parameter $a \lesssim b_{\text{crit}}$ are shown for the comparison.

Table 8. Microscopic parameters (in Ryd) for the H_4 cluster configuration (ii) calculated in the Gaussian STO-3G basis. Corresponding values of the inverse orbital size $\alpha_{\min}$ and the bond length $a_{\min}$ are provided in table 6.

b/a_0	ϵ_a^{eff}	t_1	t_2	t_3	U	K_1	K_2	K_3
1.6	−0.5352	−0.5423	−0.2986	−0.2986	1.650	0.911	0.816	0.816
2.0	−0.4511	−0.7496	−0.2230	−0.2230	1.732	0.991	0.772	0.772
2.5	−0.4863	−0.7820	−0.1451	−0.1451	1.711	0.986	0.680	0.680
3.0	−0.5221	−0.7721	−0.0923	−0.0923	1.683	0.972	0.598	0.598
3.5	−0.5467	−0.7558	−0.0571	−0.0571	1.661	0.961	0.530	0.530
4.0	−0.5613	−0.7423	−0.0342	−0.0342	1.646	0.953	0.473	0.473
5.0	−0.5715	−0.7293	−0.0115	−0.0115	1.637	0.947	0.387	0.387
6.0	−0.5719	−0.7264	−0.0038	−0.0038	1.636	0.947	0.326	0.326
8.0	−0.5692	−0.7269	−0.0003	−0.0003	1.640	0.949	0.247	0.247
10.0	−0.5685	−0.7268	−0.0000	−0.0000	1.641	0.950	0.198	0.198
20.0	−0.5673	−0.7272	−0.0000	−0.0000	1.642	0.951	0.100	0.100
∞	−0.5671	−0.7273	0	0	1.642	0.951	0	0

(i) for the planar geometry $b_{\min} = 4.00a_0$, $a_{\min} = 1.422a_0$, $\alpha_{\min} = 1.189a_0^{-1}$, and $E_G^{\min}/N = -1.1626$ Ryd; and
(ii) for the twisted 90° geometry $b_{\min} = 3.67a_0$, $a_{\min} = 1.426a_0$, $\alpha_{\min} = 1.178a_0^{-1}$, and $E_G^{\min}/N = -1.1680$ Ryd.

These values lead to the binding energies of the molecules in the nanoladders: $\Delta E_G^{(i)}/N = 20.8$ mRyd and $\Delta E_G^{(ii)}/N = 26.2$ mRyd, respectively, i.e. about three times larger than for the H_4 clusters.

One can also draw some conclusions about the nature of electronic states in those nanoladders. Namely, by calculating the so-called charge stiffness (Drude weight) and the charge gap (cf [5]) one can draw a phase diagram shown in figure 13 for a planar nanoladder on the plane a–b. For either a or b large we expect the Mott insulating state of spins $S = 1/2$. However, it is interesting to note that for bond lengths in the range 2–3 and an appropriate intermolecular distance ($b \sim a$) a quasimetalic state is possible and is followed by a band insulator for small $b < a$. The metal phase sandwiching the two, band and Mott insulating

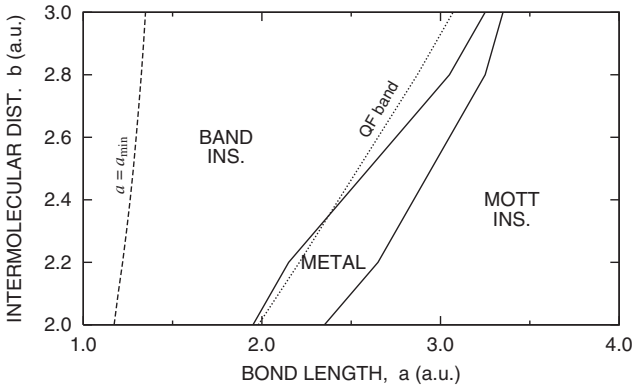

Figure 13. Phase diagram of the planar fermionic ladder. The optimal value of the bond length $a_{\min}$ is drawn as a *dashed* line. The *dotted* line marks the effective quarter-filling obtained from the noninteracting band model.

phases appears well beyond the optimal configuration for the nanoladder (see the dashed line representing $a = a_{\min}$ as a function of b). So it can appear only when a nanoladder is artificially made on a supporting substrate. The dotted line marks the model of the quarter-filled (QF) band system discussed in [5].

4. Monoatomic nanowires: from nanometal to Mott insulator

4.1. Ground-state properties

The EDABI method was applied first to nanochains starting with the Slater basis of atomic states [5, 11, 12]. In this section we present the new results starting from the STO-3G 'atomic' basis of adjustable size. The selection of this basis makes the inclusion of three- and four-site interactions possible. We limit ourselves here to the situation with one electron per atom. Strictly speaking, we study a nanochain of hydrogen atoms, which can also model the behaviour of single-valence-electron nanowires.

We start again with Hamiltonian (68) describing the so-called extended Hubbard model for a system with one orbital per atom (here the orbitals are taken as Gaussians of an adjustable size, out of which we compose the Wannier functions). The diagonalization in the Fock space is performed with the help of the Lanczos method described in detail elsewhere [5, 6]. In figure 14 we plot the ground-state energy of chains containing $N = 6$–10 hydrogen atoms, as a function of interatomic distance R (in units of a_0). The Wannier functions are calculated in the tight-binding approximation, with six attractive atomic Coulomb wells representing the periodic potential. In the inset we display the inverse size α (in units of inverse a_0) of the Gaussian functions (note that the actual size of atoms is reduced in the correlated state). The continuous $E_{\rm G}$ lines INS and M represent respectively the Mott insulating state represented by $E_{\rm G}^{\rm INS} = \epsilon_{\rm a}^{\rm eff}$, and the ideal metallic state, for which

$$E_{\rm G}^{M} = \epsilon_{\rm a}^{\rm eff} - \frac{4|t|}{\pi} + \frac{1}{2N}\sum_{i\neq j} K_{ij}\langle \delta n_i \delta n_j\rangle, \tag{70}$$

where the correlation is taken for the one-dimensional ideal gas

$$\langle \delta n_i \delta n_j\rangle = 2\frac{\sin^2(\pi|i-j|/2)}{(\pi|i-j|)^2}. \tag{71}$$

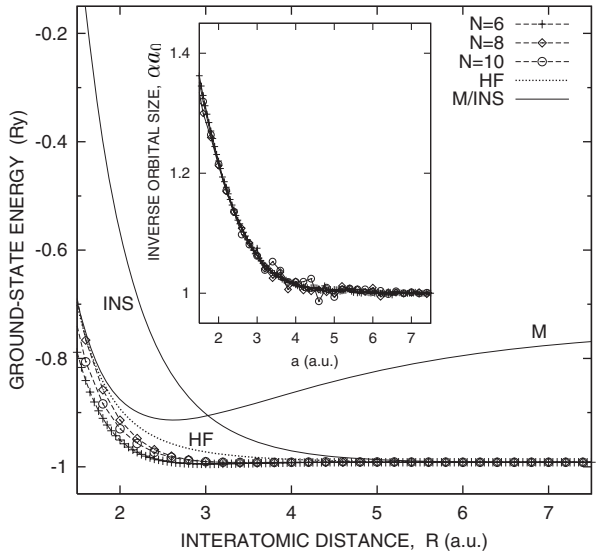

Figure 14. Ground-state energy per atom versus R for the linear chain with $N = 6$–10 atoms with periodic boundary conditions. The STO-3G Gaussian basis for representation of atomic orbitals forming the Wannier function has been used. The inset provides a universal behaviour of the inverse size α of the orbitals. For details see the main text.

For the sake of completeness, we have also included the Hartree–Fock (HF) result for $E_{\rm G}$ (the dotted line) calculated for the antiferromagnetic (Slater) state; it provides a better estimate of $E_{\rm G}$ than either M or INS curves. For discussing the HF solution we take the Hamiltonian (68) in the form

$$\begin{aligned} H^{\rm HF} = \epsilon_{\rm a}^{\rm eff} \sum_{i\sigma} n_{i\sigma} + t \sum_{i\sigma} \left(a_{i\sigma}^{\dagger} a_{i+1\sigma} + \text{h.c.} \right) \\ + U \sum_{i} \left(\langle n_{i\uparrow} \rangle n_{i\downarrow} + \langle n_{i\downarrow} \rangle n_{i\uparrow} - \langle n_{i\uparrow} \rangle \langle n_{i\downarrow} \rangle \right) \\ + \sum_{i<j} K_{ij} \left(\langle \delta n_i \rangle \delta n_j + \delta n_i \langle \delta n_j \rangle - \langle \delta n_i \rangle \langle \delta n_j \rangle \right) \\ - \sum_{i<j\sigma} K_{ij} \left(\langle a_{i\sigma}^{\dagger} a_{j\sigma} \rangle a_{j\sigma}^{\dagger} a_{i\sigma} + \langle a_{j\sigma}^{\dagger} a_{i\sigma} \rangle a_{i\sigma}^{\dagger} a_{j\sigma} - |\langle a_{i\sigma}^{\dagger} a_{j\sigma} \rangle|^2 \right). \end{aligned} \tag{72}$$

The HF solution involves calculations of the ground-state energy with a simultaneous self-consistent determination of the sublattice magnetization $m = \langle n_{i\uparrow} - n_{i\downarrow} \rangle$ and of the hopping correlation function $\langle a_{i\sigma}^{\dagger} a_{j\sigma} \rangle$, which will not be discussed in detail here [5] (obviously, $\langle \delta n_i \rangle = 0$).

The most spectacular are the spin–spin correlations in the collective spin singlet ($\sum_{i=1}^{N} \mathbf{S}_i \equiv 0$) state. In figure 15(a) we display the corresponding spin–spin correlation function $\langle \mathbf{S}_i \cdot \mathbf{S}_j \rangle$ as a function of the distance $|i - j|$ for $N = 10$ and several values of R. We observe Néel-like state correlations in this spin singlet state as it oscillates through the whole system length. For $N = 11$ these quasi-oscillatory correlations are strongly suppressed due to the spin-frustration effects, as shown explicitly in figure 15(b). Changing the lattice constant R does not alter the picture qualitatively. This long-range feature of spin–spin correlations will have profound consequences on the single-particle spectrum, as we discuss below. Here the boundary conditions discussed below (cf section 4.5) have been considered, although the

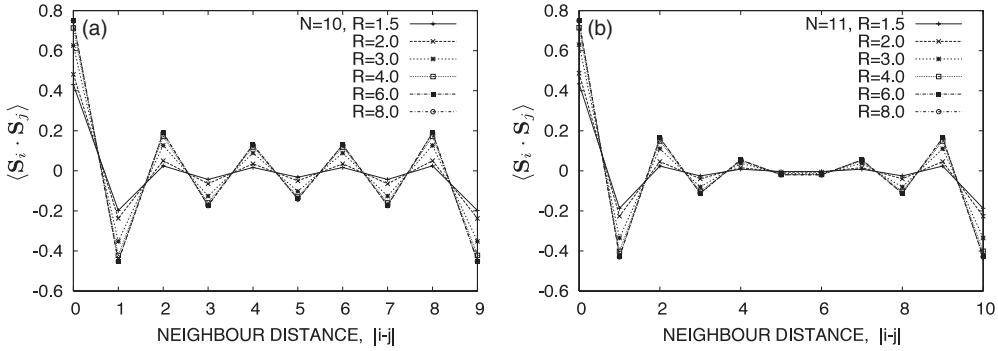

Figure 15. Parity effect on spin ordering: spin–spin correlations for nanochains of $N = 10$ (a) and $N = 11$ (b) atoms. The values of the interatomic distance R are specified in the atomic units ($a_0 = 0.529$ Å).

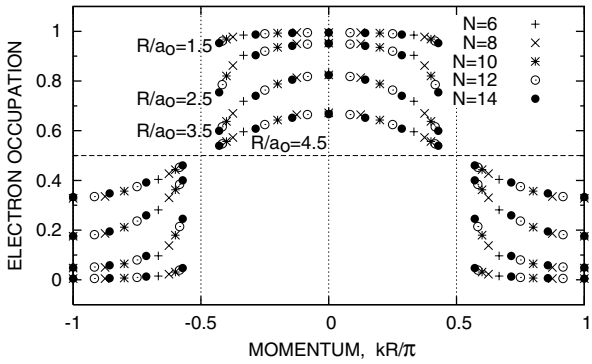

Figure 16. Momentum distribution $\overline{n}_{\mathbf{k}\sigma}$ for the number of atoms $N = 6$–14 as it evolves with the increasing lattice constant R.

difference between cases a and b survives even for the periodic boundary conditions. Additional features of the N dependence of $\langle \mathbf{S}_i \cdot \mathbf{S}_j \rangle$ have been discussed in [21].

4.2. Momentum distribution in the ground state: Fermi or Luttinger nanoliquid localization?

We now introduce the particle quasi-momentum distribution $n_{\mathbf{k}\sigma}$ in the ground state for the situation with one electron per atom; this is displayed in figure 16 for the number of atoms $N = 6$–14. We observe a very universal character of the curves provided the periodic boundary conditions are taken for the chains of $N = 4n + 2$ atoms, whereas the antiperiodic boundary conditions are taken for $N = 4n$ atoms, with n being a natural number. It is very tempting to regard the distributions for $R/a_0 \leqslant 3.5$ as a modified Fermi–Dirac function characterizing the Fermi liquid even for such short chains for which we have discrete momentum states. However, for $R/a_0 \to 4$ the distributions becomes continuous, i.e. without an apparent Fermi ridge at Fermi momentum $k_{\mathrm{F}} = \pi/(2R)$, in rough agreement with the preliminary results for the case with the Slater-type orbitals [12]. So, a crossover with increasing interatomic distance from the Fermi-liquid-like behaviour to the chain of atomic-like states is clearly seen. It should be noted that the Luttinger-liquid-like scaling fitting to the points displayed in figure 16 is equally convincing, at least for this half-filled band configuration, as discussed next.

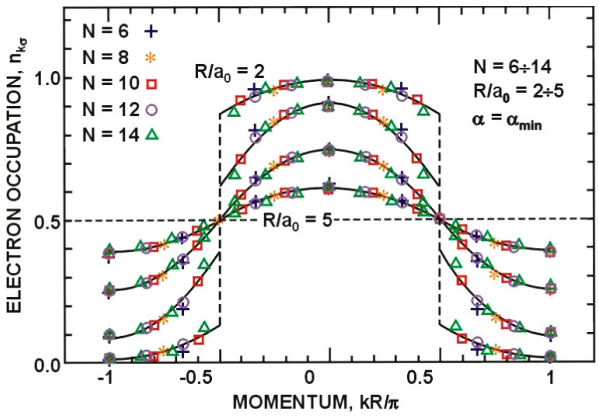

Figure 17. Statistical distribution $n_{\mathbf{k}\sigma}$ for electrons in a chain of $N = 6$–14 atoms with periodic boundary conditions. The interatomic distance R is specified in units of Bohr radius a_0. The continuous line represents the parabolic interpolation, which is of the same type for both $k > k_F$ and $k < k_F$.

4.3. Single-particle spectral density function evolution

The state of a nanochain viewed through the statistical distribution of momentum states can be discussed as follows. The ideal Mott localized state, as is seen in the bulk systems, is not possible for a finite system. This is simply because the length of the system is finite and therefore the probability of the electron tunnelling from an atomic state on one chain end to the other end is *nonzero*. The quantitative question is whether it is of the order of $e^{-N\alpha R}$ or larger. Due to the fact that the overlap integral is $\sim\frac{1}{3}(\alpha R)^2 e^{-\alpha R}$, the probability is enhanced by a nonzero hopping amplitude between more distant neighbours. Having in mind this circumstance, it is at least imaginable that the distribution function displayed in figure 16 is Fermi–Dirac-like for $\alpha R \sim 1$. One can thus try to formalize this observation further. Namely, in figure 17 we plot $n_{\mathbf{k}\sigma}$ for a half filled band system containing up to $N = 14$ electrons. The continuous lines represent the parabolic parametrization:

$$n_{\mathbf{k}\sigma} = \tfrac{1}{2}\mathrm{sgn}(k - k_F)\left[\alpha(k - k_F)^2 + \beta|k - k_F| + \gamma\right], \tag{73}$$

for both $k < k_F$ and $k > k_F$ (note that the Fermi point is not occupied for N even). This parametrization, in fact implying a discontinuous distribution, allows us to interpret the distribution discontinuity $\Delta n_{k_F} \equiv n_{k_F-0} - n_{k_F+0}$ in terms of effective mass enhancement at the Fermi point.

$$m_F^*/m_{\mathrm{BAND}} = (\Delta n_{k_F})^{-1} \equiv Z^{-1}, \tag{74}$$

where Z^{-1} is the usual Fermi-liquid enhancement factor. The corresponding enhancement factor determined in this manner is plotted in figure 18 (squares), whereas the solid line represents the finite-size scaling with interatomic distance, $m_F^*/m_{\mathrm{BAND}} = A|R - R_C|^{-\gamma}$, with $A \simeq 10.2$, the localization thereshold is $R_C a_0 = 3.92$, and the critical exponent has the approximate value $\gamma = 4/3$. This behaviour emulates a quantum critical behaviour and should not be taken literally. Nonetheless, the value of R_C distinguishes *qualitatively* between the nanometallic state $R < R_C$ (for which the distribution (73) has a jump at k_F) and the Mott insulating (semiconducting) state ($R > R_C$; the distribution function is a continous function of k).

However, the situation is not this simple. One can ask the question of whether this short one-dimensional system does not rather resemble the Luttinger-liquid-like behaviour. This

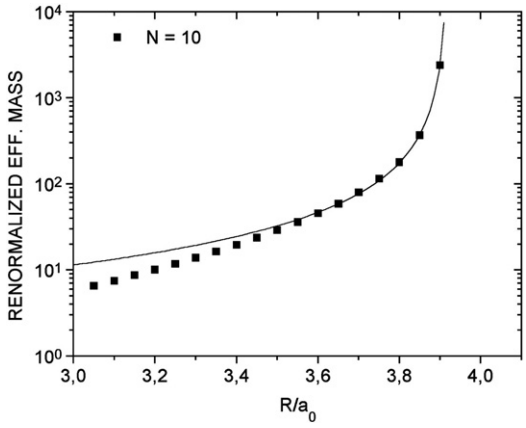

Figure 18. The critical behaviour of the quasiparticle mass at the Fermi level; for details see the main text.

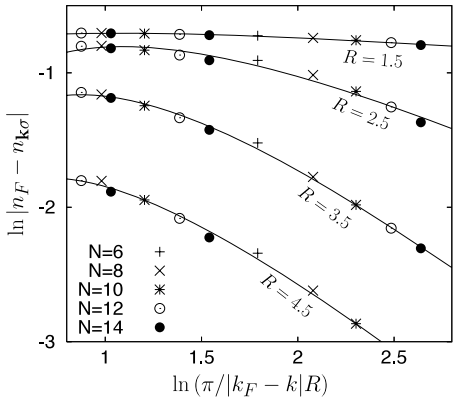

Figure 19. Luttinger-liquid scaling for a half-filled one-dimensional chain of $N = 6$–14 atoms. Interatomic distance R is specified in the units of a_0.

task has been undertaken seriously and in figure 19 we plot the fitting of the data displayed in figure 16 to the corresponding dependence for the Tomanaga–Luttinger liquid, with the logarithmic correction included, namely [22]

$$\ln |n_{k_\mathrm{F}} - n_{k\sigma}| = -\Theta \ln z + b \ln \ln z + c + \theta(1/\ln z), \tag{75}$$

where $z = \pi/|k_\mathrm{F} - \pi/R|$, Θ, b, and c are constants. The parameters depend on the distance R, as shown elsewhere [22]. This fitting also provides the localization thereshold $R_C \simeq 2.60 a_B$, which is reduced by 50% from the value for the Fermi liquid interpretation of $n_{k\sigma}$. One should also note that the present interpretation of the exact solution displayed in figure 16 does not admit a discontinuity at $k = k_\mathrm{F}$. However, it is quite amazing that both the Fermi- and Luttinger-liquid interpretations can provide a satisfying interpretation of $n_{k\sigma}$ to an equal degree. This means that there must be an underlying universal behaviour of a new type, incorporating Fermi- and Luttinger-liquid concepts, at least semiquantitatively. Nonetheless, for the not too large R the Fermi–Dirac-like distribution fits better the k dependence. The situation for odd N requires an explicit discussion of boundary conditions and is provided below.

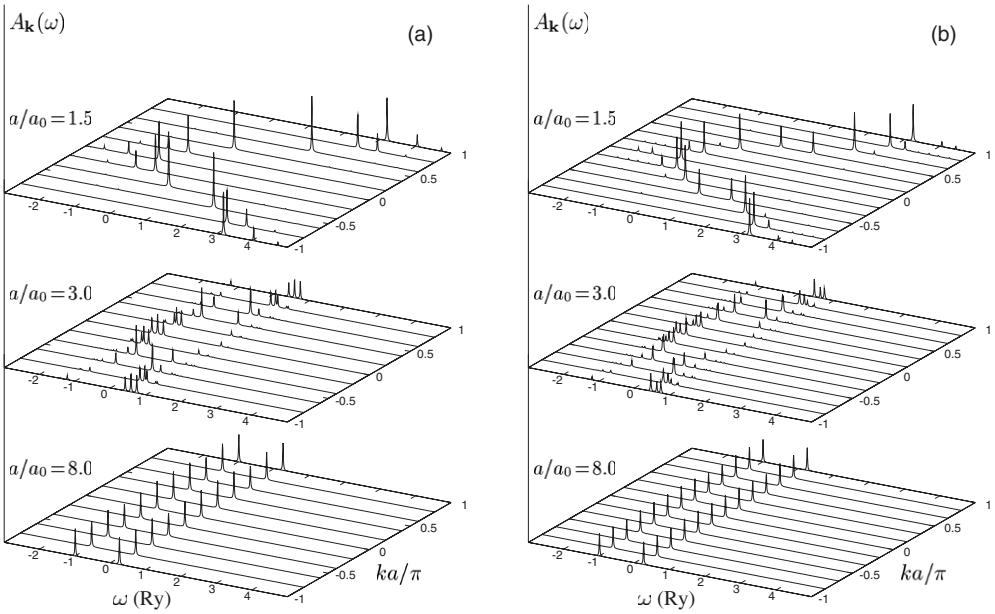

Figure 20. Spectral functions $A(\mathbf{k}, \omega)$ for $N = 10$ (a) and $N = 12$ atoms, with periodic boundary conditions. A clear dispersion of the states is observed for $R = 1.5a_0$, which transform into the atomic peaks with the increasing R, through an incoherent regime for $R/a_0 \approx 3$.

To characterize the spectrum of single-particle excitations we use the definition of the spectral-density function

$$A(\mathbf{k}, \omega) = \sum_n \left| \langle \Phi_n^{N\pm1} | a_{\mathbf{k}\sigma}^{\dagger} | \Phi_0^N \rangle \right|^2 \delta \left[\omega - (E_n^{N+1} - E_0^N) \right], \tag{76}$$

where the upper(lower) sign corresponds to the energies with $\omega > \mu$ ($\omega < \mu$), respectively, $|\Phi_n^N\rangle$ is the nth eigenstate of the system containing N particles, E_n^N is the corresponding eigenenergy, and $\langle \cdots \rangle$ is the matrix element are calculated within the Lanczos algorithm [23, 24, 27]. In figure 20 we present the panel of $A(\mathbf{k}, \omega)$ for three distances R. For small R, a clear two-peak structure appears at the Fermi momenta $k_{\mathrm{F}} = \pm\pi/(2R)$ for $N = 12$; an artificial broadening of the peaks appears because we use the approximate expression for the $\delta(x)$ function: $\delta(x) \approx (1/\pi)\epsilon/(x^2 + \epsilon^2)$, with $\epsilon = 10^{-2}$ Ryd. The splitting is caused by the antiferromagnetic correlations depicted in figure 15(a). In the range $R/a_0 \leqslant 2$ the quasiparticles are well defined, but an incoherent part grows with the increasing R. For $R/a_0 \sim 3$–4 the *Hubbard subbands* are formed and evolve continuously into atomic levels located respectively at $\omega = \epsilon_{\mathrm{a}}$ and $\omega = \epsilon_{\mathrm{a}} + U$ for $R \to \infty$. These two limiting peak positions correspond to the ground H^0 and excited H^- states, respectively. Combining the last results with the corresponding discussion for the H_N clusters, one sees that *the Hubbard subband structure represents a universal feature of nanoscopic systems*. In the limit of larger interatomic separation this structure is clearly distinguishable from the discrete level structure coming from geometric quantization of this confined system.

To demonstrate the importance of the *incoherent* part of the spectrum we have calculated the density of states $\mathcal{N}(\omega) = \sum_{\mathbf{k}} A(\mathbf{k}, \omega)$, displayed in figure 21 for $N = 10$ atoms, for the interatomic distances specified. In the regime $R = 3$–$5a_0$ well resolved quasiparticle peaks coalesce into a complicated random-like (incoherent) spectrum, out of which clean atomic

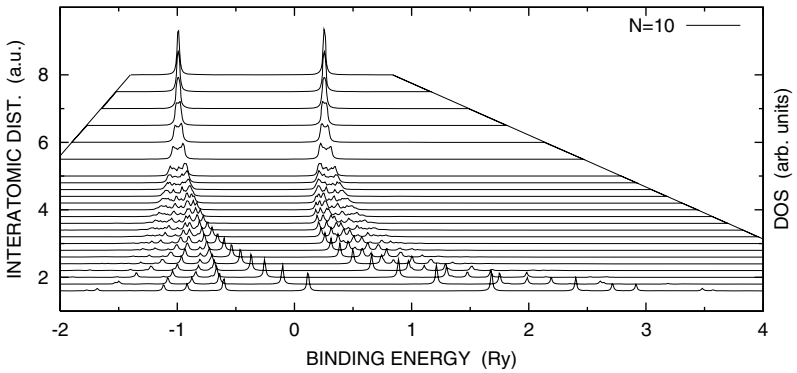

Figure 21. Density of single-particle states for $N = 10$ atoms. Note a pronounced incoherent spectrum for R in the range 3–5a_0.

Table 9. Optimized inverse orbital size, microscopic parameters and the ground-state energy for $N = 10$ atoms calculated in the Slater-type basis, as a function of interatomic distance. Intersite Coulomb repulsion K_1 is included on the mean-field level in $\epsilon_a^{\rm eff}$; the Hubbard U term is treated exactly. The single-particle potential contains *six* Coulomb wells.

R/a_0	$\alpha_{\rm min}a_0$	$\epsilon_a^{\rm eff}$	t	U	K	E_G/N
1.5	1.806	0.9103	−1.0405	2.399	1.695	0.0665
2.0	1.491	−0.1901	−0.5339	1.985	1.172	−0.5179
2.5	1.303	−0.6242	−0.3076	1.722	0.889	−0.7627
3.0	1.189	−0.8180	−0.1904	1.553	0.713	−0.8800
3.5	1.116	−0.9104	−0.1230	1.440	0.596	−0.9391
4.0	1.069	−0.9559	−0.0815	1.365	0.513	−0.9693
4.5	1.039	−0.9784	−0.0546	1.317	0.451	−0.9848
5.0	1.022	−0.9896	−0.0370	1.288	0.403	−0.9926
6.0	1.013	−0.9977	−0.0165	1.269	0.334	−0.9982
7.0	1.001	−0.9995	−0.0072	1.252	0.286	−0.9996
8.0	1.001	−0.9999	−0.0031	1.251	0.250	−0.9999
10.0	1.000	−1.0000	0.0003	1.250	0.200	−1.0000

peaks emerge for larger R. Note that the intermediate regime corresponds to the situation for which the bare bandwidth $W = 4|t|$ of the single-particle states fulfils the condition $W \sim U$, i.e. the electronic system switches from the weak- to the rather strong-correlation regime, corresponding to the delocalization–localization crossover of the Mott–Hubbard type taking place. For one electron per atom the lower energy manifold is filled with electrons, whereas the upper is empty. The presence of the incoherent spectrum for $R \approx 3$–$5a_0$ also seems to represent a universal feature, as it also appears for larger values of N.

4.4. Slater versus Gaussian trial basis

We now compare the results obtained within EDABI when either the adjustable Slater or the STO-3G functions are used. Probably, most interesting is to compare the results for the Hubbard model with intersite Coulomb interactions taken in the Hartree–Fock approximation (only then are the results for the Slater 1s-like basis energetically stable. In table 9 we list the results for the Slater basis containing both E_G and microscopic parameters for a ring of

Table 10. The same as in table 9, calculated in the Gaussian-type STO-3G basis.

R/a_0	$\alpha_{\min}a_0$	$\epsilon_{\rm a}^{\rm eff}$	t	U	K	$E_{\rm G}/N$
1.5	1.309	0.1311	−0.8643	2.002	1.154	−0.5684
2.0	1.205	−0.5342	−0.4595	1.718	0.908	−0.8154
2.5	1.120	−0.7893	−0.2750	1.530	0.750	−0.9139
3.0	1.067	−0.8975	−0.1776	1.412	0.639	−0.9567
3.5	1.038	−0.9465	−0.1197	1.342	0.558	−0.9756
4.0	1.020	−0.9698	−0.0820	1.299	0.494	−0.9841
4.5	1.013	−0.9812	−0.0562	1.276	0.442	−0.9881
5.0	1.005	−0.9868	−0.0382	1.260	0.399	−0.9901
6.0	1.003	−0.9908	−0.0170	1.251	0.333	−0.9914
7.0	1.000	−0.9915	−0.0072	1.247	0.286	−0.9917
8.0	1.000	−0.9917	−0.0027	1.246	0.250	−0.9917
10.0	1.000	−0.9917	−0.0003	1.246	0.200	−0.9917

Table 11. The same as in table 9, calculated in the Gaussian-type STO-3G basis, with the inclusion of the *long-range* Coulomb interactions.

a/a_0	$\alpha_{\min}a_0$	$\epsilon_{\rm a}^{\rm eff}f$	t	U	K	$E_{\rm G}/N$
1.5	1.322	0.1340	−0.8684	2.014	1.156	−0.7691
2.0	1.208	−0.5338	−0.4603	1.721	0.909	−0.9377
2.5	1.119	−0.7894	−0.2748	1.528	0.749	−0.9824
3.0	1.063	−0.8977	−0.1770	1.407	0.639	−0.9924
3.5	1.030	−0.9466	−0.1192	1.334	0.557	−0.9932
4.0	1.011	−0.9697	−0.0817	1.288	0.493	−0.9922
4.5	1.006	−0.9812	−0.0562	1.269	0.442	−0.9917
5.0	1.006	−0.9868	−0.0382	1.260	0.399	−0.9915
6.0	1.002	−0.9908	−0.0170	1.250	0.333	−0.9917
7.0	1.000	−0.9915	−0.0072	1.247	0.286	−0.9917
8.0	1.000	−0.9917	−0.0027	1.246	0.250	−0.9917
10.0	1.000	−0.9917	−0.0003	1.246	0.200	−0.9917

$N = 10$ atoms. The same for the case of the STO-3G basis is shown in table 10. One sees that the Gaussian basis provides a lower value of $E_{\rm G}$. This is because in the Slater case we have neglected three- and four-site interactions in the atomic basis, that represents a rather crude approximation. In contrast, the results for $E_{\rm G}$ obtained for the STO-3G basis for $N = 10$ atoms are very close (within 10^{-2} Ryd) to those obtained for an exact solution for an infinite chain [25] and the values of the microscopic parameters within 10^{-3} [23]. Because of the good accuracy of the results for the Gaussian basis we have also provided in table 11 the results for the chain of $N = 10$ atoms when the long-range parts of the Coulomb interactions $\sim K_{ij}$ are included. These results provide the range of variation of the microscopic parameters when compared to either H_2 (cf table 2) or the U_1 value for the He atom (cf table 3).

4.5. The role of boundary conditions: parity effects

It is believed that system properties in the thermodynamic limit ($N \to \infty$) are the same regardless of the boundary conditions used. This claim has been tested on many model systems. However, for finite clusters the boundary conditions are crucial. For the chains studied here when $N = 4n + 2$ (where n is a natural number) the periodic boundary conditions (PBCs) are used, whereas for $N = 4n$ the antiperiodic boundary conditions (ABCs) lead to a lower-energy

state. Namely, the terminal-atomic annihilation operators should be defined as follows:

$$\begin{aligned} a_{N+1,\sigma} &\to a_{1\sigma} \qquad \text{for PBC,} \\ a_{N+1,\sigma} &\to -a_{1\sigma} \qquad \text{for ABC.} \end{aligned} \tag{77}$$

Therefore, the terminal hopping term involving the end atoms changes sign for ABC, while the interaction terms $\sim n_{i\uparrow}n_{i\downarrow}$, $n_i n_j$ and $\mathbf{S}_i \cdot \mathbf{S}_j$ remain unaltered. Obviously, the periodic boundary conditions are appropriate for any N when we have a ring geometry. The situation becomes more involved when N is an odd number. Namely, we write down the Hamiltonian (68) in the form

$$H = \epsilon_{\mathrm{a}}^{\mathrm{eff}} \sum_{i\sigma} n_{i\sigma} + t \sum_{j\sigma} \mathrm{e}^{-\mathrm{i}\Phi/N} a_{j\sigma}^{\dagger} a_{j+1\sigma} + U \sum_{i} n_{i\uparrow} n_{i\downarrow} + \sum_{i<j} K_{ij} \delta n_i \delta n_j, \tag{78}$$

where Φ is the fictitious (dimensionless) flux through the ring. One can show that the unitary transformation $c_{j\sigma} \to \mathrm{e}^{-\mathrm{i}\Phi/N} c_{j\sigma}$ allows for accumulation of a complex phase factor in the terminal hopping term, which then takes the form $t(\mathrm{e}^{-\mathrm{i}\Phi} a_{N\sigma}^{\dagger} a_{1\sigma} + \text{h.c.})$, and this can be regarded as the generalized boundary condition $a_{N+1\sigma} \to \mathrm{e}^{\mathrm{i}\Phi/N} a_{1\sigma}$. We do not distinguish between the system with a fictitious flux and the generalized boundary conditions. The presence of the flux can be regarded as an accumulation of the Berry phase during the motion of an individual electron in the milieu of all other electrons. With such an interpretation the boundary conditions also apply to a linear chain.

The electron momentum for nanochains with such boundary conditions is displayed in figure 23. The discrete momenta, corresponding to the solution of the single-particle part of (78) for a finite N, are given by

$$k_n = \frac{2\pi n - \Phi}{N}, \qquad 0 \leqslant n \leqslant N. \tag{79}$$

The optimal BCs, corresponding to the minimal ground-state energy E_{G}, with respect to Φ, are realized for $\Phi = 0$ when $N = 6, 10, 14, \ldots$ (periodic BCs), $\Phi = \pi$ when $N = 4, 8, 12, \ldots$ (antiperiodic BCs), and $\Phi = \pi/2, 3/2\pi$ when N is odd. A basic analysis of equation (78) shows that, for the optimal BCs, the Fermi momentum value $k_{\mathrm{F}} = \pi/(2R)$ is never reached for even N, whereas for odd N it happens for a single value of n. This circumstance has an important implication for the nanochain electronic structure; however, it almost does not affect its transport properties, as discussed below. The exact meaning of the averaging procedure when drawing figure 23 is elaborated elsewhere. Analogously, the effect of BCs on the spin–spin correlation function $\langle \mathbf{S}_i \cdot \mathbf{S}_j \rangle$ is also touched upon there.

An explicit form of the dispersion relation derived from the spectral density functions with inclusion of the generalized boundary conditions is shown in figure 22. We see again that the spin splitting is present. Also, one can see the difference between either the dispersion relation for noninteracting particles or with that calculated in the Hartree–Fock approximation for the Slater antiferromagnetic chain.

5. Transport in nanosystems

In this section we complement the discussion of nanochains by providing the values of Drude weight (charge stiffness) and optical gap. We also show how the EDABI method can be used to calculate the conductance of an open system: a quantum dot attached to the leads.

5.1. Drude weight for nanochains

The real part of the optical conductivity at zero temperature is determined by the corresponding real part of the linear response to the applied electric field [26], and can be written as

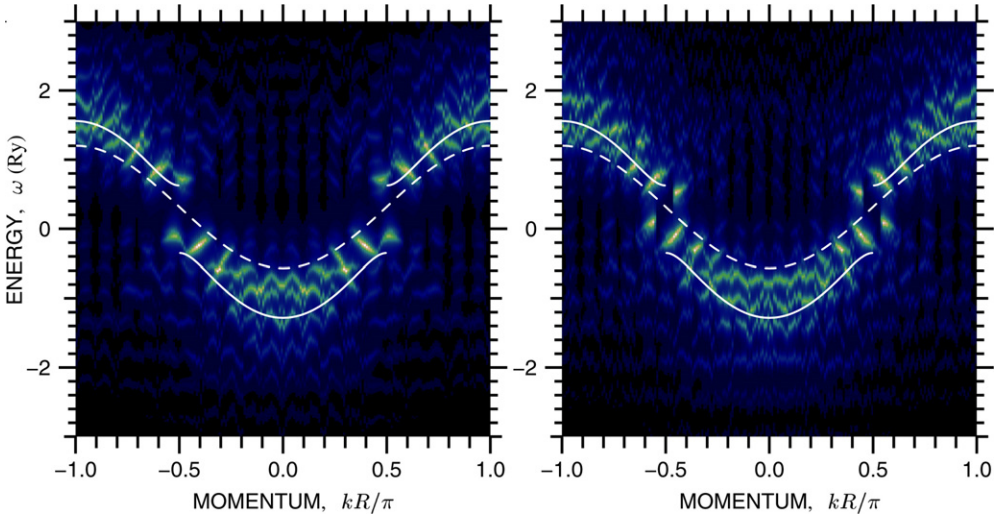

Figure 22. Spectral-density-peak positions for the nanochain of $N = 10$ (*left* panel) and $N = 11$ (*right* panel) atoms with generalized boundary conditions. The Hartree–Fock (*solid* line) and noninteracting system (*dashed* line) dispersion relations are shown for comparison.

$\sigma(\omega) = D\delta(\omega) + \sigma_{\rm reg}(\omega)$, where the regular part is

$$\sigma_{\rm reg}(\omega) = \frac{\pi}{N}\sum_{n\neq 0}\frac{\left|\langle\Psi_n|\, j_p\,|\Psi_0\rangle\right|^2}{E_n - E_0}\delta\left(\omega - (E_n - E_0)\right), \tag{80}$$

whereas the Drude weight (the *charge stiffness*) D is defined by

$$D = -\frac{\pi}{N}\langle\Psi_0|\, T\,|\Psi_0\rangle - \frac{2\pi}{N}\sum_{n\neq 0}\frac{\left|\langle\Psi_n|\, j_p\,|\Psi_0\rangle\right|^2}{E_n - E_0}, \tag{81}$$

where the kinetic-energy term T is the same as the second term in equation (78), and the diamagnetic current operator is defined as usual: $j_p = it\sum_{j\sigma}(a^\dagger_{j\sigma}a_{j+1\sigma} - \text{h.c.})$. Here the states $|\Psi_n\rangle$ in equations (80) and (81) are the eigenstates of the Hamiltonian (78) corresponding to the eigenenergies E_n, again with boundary conditions which minimize the ground-state energy for a given system size N (see the previous section). We calculate matrix elements $\langle\Psi_n|\, j_p\,|\Psi_0\rangle$ numerically by adapting the method developed by Dagotto [27], which is stable for an *even* number of electrons only. Namely, we diagonalize the Hamiltonian (78) in the Fock space with the help of the Davidson technique [28], and then repeat the procedure starting from a specially prepared initial state $j_p\,|\Psi_0\rangle$. Replacing the Lanczos scheme, utilized in [27], by the Davidson one provides an excellent accuracy for either *even* or *odd* number of electrons. The evolution of Drude weight with N and R is shown in figure 24. In the half-filled case $N_e = N$ (cf figure 24(a)) Drude weight gradually decreases with N, as we have shown for even N [29]. The most interesting feature of these results is that the curves for odd N fit smoothly between those for even N, with very weak parity effect, totally incomparable with that present in the charge gap and electron momentum distribution [30]. This observation can be understood when we take into account that the Drude weight defined by equation (81) is the *integral* quantity, involving the summation over all the excited states of the Hamiltonian equation (78), so it cannot be determined only by the electronic structure near the Fermi points, particularly for a small system.

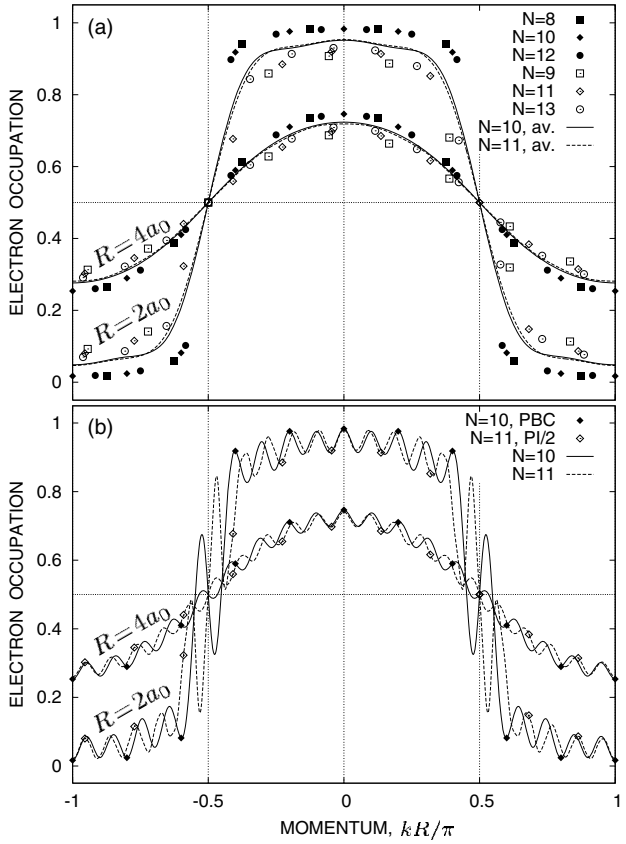

Figure 23. Electron momentum distribution for chains of $N = 8$–13 atoms: (a) datapoints for *optimal* boundary conditions (BCs) and the sample $n(k)$ curves averaged over BCs (*solid* lines); (*b*) the original $n(k_q(\phi))$ functions used for the averaging.

The parity effect on Drude weight disappears for the system with a single hole ($N_e = N - 1$, cf figure 24(b)), in which the magnetic frustration is absent. For this case, the Drude weight evolution with R is very interesting. In the weak-correlation range ($R/a_0 \lesssim 2$) the chain shows a highly conducting behaviour for each N. Next, in the intermediate range ($R/a_0 = 4$–5) the Drude weight decreases rapidly with N, indicating an insulating (Mott–Hubbard) state in the large-N limit. In the strongly correlated range ($R/a_0 \sim 10$) the Drude weight again approaches its maximal value $D = 1$. Such a behaviour can be explained when we analyse the situation in two steps. *First,* for low values of R, the bandwidth-to-interaction ratio is small, and the system with a single hole does not differ significantly from a half-filled one. This is why in both cases Drude weight decreases gradually with both N and R, as the tunnelling amplitude through the barrier of a finite width. *Second*, for the largest values of R, the system can be described by an effective t–J model [31] with a coupling constant $J = 4t^2/(U - K) \ll |t|$ (where $K \equiv K_{j,j+1}$ denotes the nearest neighbour Coulomb repulsion), which corresponds to an asymptotically free hole motion. Then, it become clear that in the intermediate range the Drude weight has to be suppressed, which can be interpreted in terms of a partially localized spin-ordered state. It would be very interesting to test experimentally this result, possibly for a mesoscopic atomic ring.

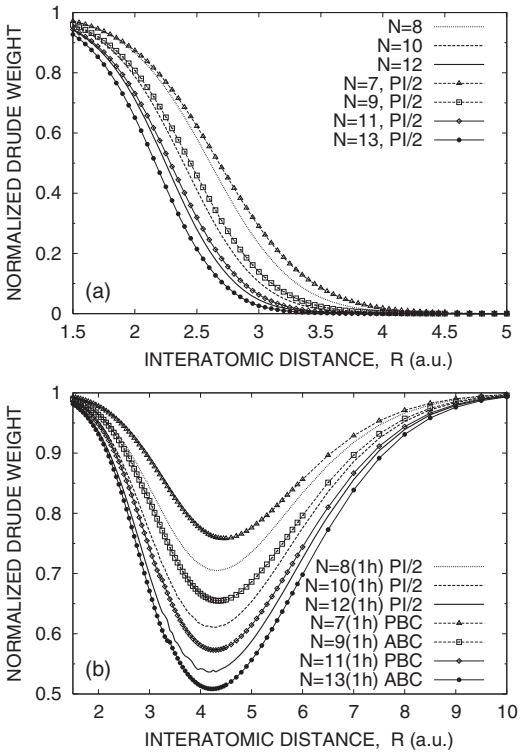

Figure 24. Normalized Drude weight for nanochains in the *half-filled* case (a), and for a system with a single hole (b). The *optimal* boundary conditions are specified for each dataset.

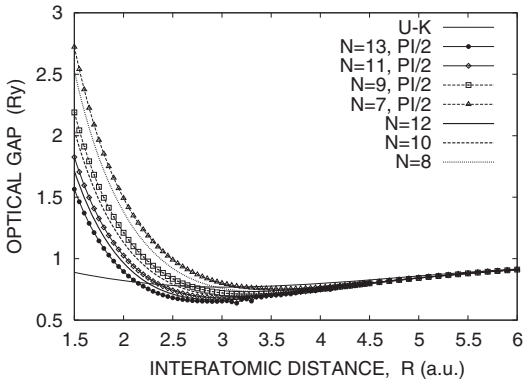

Figure 25. Optical gap for nanochains in the *half-filled* case.

The smooth behaviour of the system transport properties with N is illustrated in figure 25 on the example of another relevant quantity, the *optical gap* $\Delta E_{\rm opt} = E_i - E_0$ (where E_i is the energy lowest-lying excited level $|\Psi_i\rangle$, for which $\langle\Psi_i|j_p|\Psi_0\rangle \neq 0$). Again, adding a single hole totally removes the weak parity effect (not shown). The large-R behaviour of $\Delta E_{\rm opt}$ could be explained by the value for an insulating limit $\Delta E_{\rm opt} \approx U - K$, whereas for small R we have a

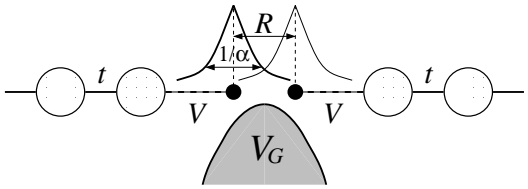

Figure 26. Diatomic molecule as a double quantum dot.

strong N dependence similar to those observed for D. The latter shows that the contribution of the state $|\Psi_i\rangle$ to the sum (81) is dominant for such a *partly localized* quantum nanoliquid [29].

5.2. H_2 molecule as a quantum dot

We have recently shown that the EDABI method is useful to investigate the zero-temperature conductance of a diatomic molecule, modelled as a correlated double quantum dot attached to noninteracting leads [4]. This became possible when utilizing the Rejec–Ramšak formulae, relating the linear-response conductance to the ground-state energy dependence on magnetic flux [32]. Here we complement the discussion with the stability analysis showing that large coupling between molecule and the leads may provide the possibility for interatomic distance manipulation in an experiment.

We start with the Hamiltonian, which is a generalization of the Anderson impurity model [33], and can be written as

$$H = H_L + V_L + H_C + V_R + H_R, \tag{82}$$

where H_C models the central region, $H_{L\,(R)}$ describes the left (right) lead, and $V_{L\,(R)}$ is the coupling between the lead and the central region. Both $H_{L\,(R)}$ and $V_{L\,(R)}$ terms have a tight-binding form, with the hopping t and the tunnelling amplitude V

$$H_{L\,(R)} = t \sum_{j \neq L\,(R),\sigma} (a^{\dagger}_{j\sigma} a_{j+1,\sigma} + \text{h.c.}), \tag{83}$$

$$V_{L\,(R)} = V \sum_{\sigma} (a^{\dagger}_{L\,(R)\sigma} a_{1(2)\sigma} + \text{h.c.}), \tag{84}$$

as depicted schematically in figure 26. The index $j = L\ (R)$ corresponds to the last atom of the left (right) lead. The central-region term H_C is a version of Hamiltonian (68) for two atoms, and describes a double quantum dot with electron–electron interaction

$$H_C = (\epsilon_{\text{a}} - eV_{\text{G}}) \sum_{j=1,2} n_i - t' \sum_{\sigma=\uparrow,\downarrow} (a^{\dagger}_{1\sigma} a_{2\sigma} + \text{h.c.}) + U \sum_{j=1,2} n_{i\uparrow} n_{i\downarrow} + K n_1 n_2 + (Ze)^2/R, \tag{85}$$

where ϵ_{a} is atomic energy, V_{G} is an external gate voltage, t' is the internal hopping integral, U and K represent the intra- and inter-site Coulomb interactions, respectively, and the last term describes the Coulomb repulsion of the two ions at the distance R. Here we put $Z = 1$ and calculate all the parameters ϵ_{a}, t', U, and K as the Slater integrals [34] for 1s-like hydrogenic orbitals $\Psi_{1\text{s}}(\mathbf{r}) = \sqrt{\alpha^3/\pi}\exp(-\alpha|\mathbf{r}|)$, where α^{-1} is the orbital size (cf figure 26). The parameter α is optimized to get a minimal ground-state energy for the whole system described by the Hamiltonian (82). Thus, following the idea of the EDABI method [29], we reduce the number of physical parameters of the problem to just three: the interatomic distance R, the gate voltage V_{G}, and the lead–molecule coupling V (we put the lead hopping $t = 1$ Ryd $= 13.6$ eV to work in the wide-bandwidth limit).

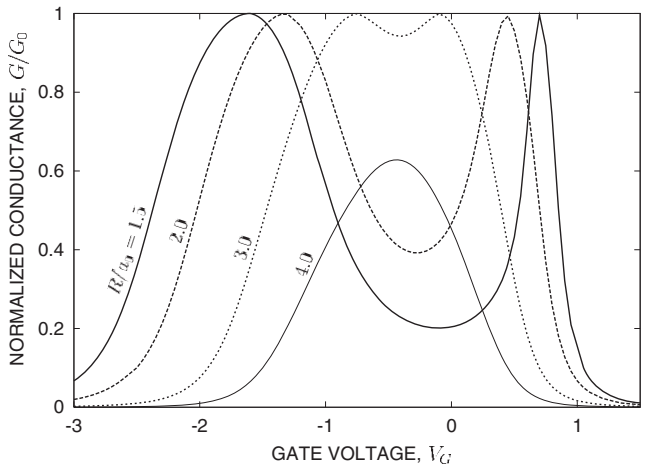

Figure 27. Zero-temperature conductance of the system in figure 26 as a function of the gate voltage V_G and interatomic distance R. 1s orbital size α^{-1} is optimized variationally. The lead parameters are $t = 1$ Ryd and $V = 0.5t$.

We discuss now the molecule conductivity calculated from the Rejec–Ramšak two-point formula [32]:

$$G = G_0 \sin^2 \pi [E(\pi) - E(0)]/2\Delta, \tag{86}$$

where $G_0 = 2e^2/\hbar$ is the conductance quantum, $\Delta = 1/N\rho(\epsilon_F)$ is the average level spacing at Fermi energy, determined by the density of states in an infinite lead $\rho(\epsilon_F)$, and $E(\pi)$ and $E(0)$ are the ground-state energies of the system with periodic and antiperiodic boundary conditions, respectively. $E(\phi)$ is calculated for $\phi = 0, \pi$ within the Rejec–Ramšak variational method [32], complemented by the inverse orbital size α optimization, as mentioned above. We use typically $N = 10^2$–10^3 sites to reach convergence.

In figure 27 we show the conductivity for $V = 0.5t$, and different values of the interatomic distance R. The conductance spectrum evolves from the situation of well separated peaks corresponding to the independent filling of bonding and antibonding molecular orbitals ($R \lesssim 2a_0$, where a_0 is the Bohr radius), to the single peak in the intermediate range ($R \approx 3a_0$), which decays when $t' \ll V$ for large R.

Probably, the most interesting feature of the conductance depicted in figure 27 is their strong asymmetry for small R. Namely, the low-V_G conductance peak, corresponding to the system filling $\langle n_1 + n_2 \rangle \approx 1$ (one *hole*) is significantly wider than the high-V_G peak for $\langle n_1 + n_2 \rangle \approx 3$ (one *extra electron*). Such a particle–hole symmetry breaking is the novel feature, observed when including the correlation-induced basis optimization, and absent in the parametrized-model approach [32, 35]. It is also a new feature of a nanosystem, not observed in mesoscopic double quantum dots [36], where the particle–hole symmetry holds.

The relation between the observed asymmetry, basis renormalization, and electron correlations can be clarified as follows. *First*, one can observe that the optimal values of the variational parameter α, provided in figure 28(a), decrease dramatically for high V_G, corresponding to the overdoped situation $\langle n_1 + n_2 \rangle > 2$ (cf figure 28(b)). This is because the system minimizes the energy of double occupancies, which is of the order $U \sim \alpha$ [34]. *Then*, we focus on an small R limit, in which the good separation of molecular orbitals allows

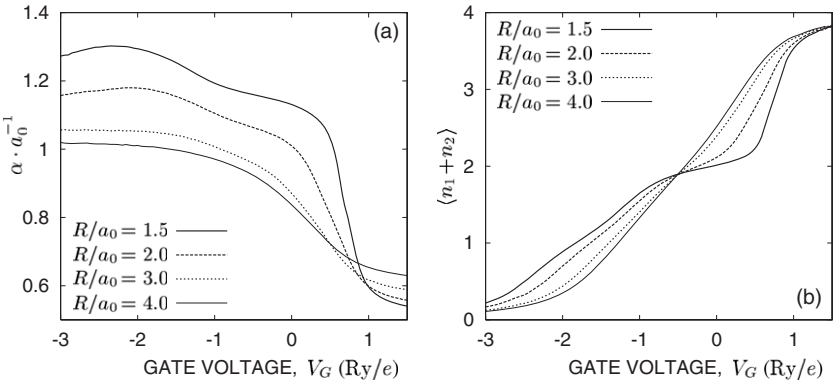

Figure 28. The optimized inverse inverse orbital size (a) and average central region occupancy (b) for the diatomic molecule attached to noninteracting leads characterized by the parameters $t = 1$ Ryd and $V = 0.5t$.

Table 12. The binding energy ΔE and the bond length $R_{\min}$ for different couplings to the lead V. The conductance at the energy minimum is also provided.

V/t	ΔE	$R_{\min}/a_0$	$G_{\min}^{V_G=0}/G_0$
0.0	−0.296	1.43	0
0.1	−0.293	1.44	10^{-4}
0.2	−0.282	1.46	0.004
0.3	−0.180	1.52	0.023
0.4	−0.040	1.59	0.093
0.5	+0.074	1.93	0.422

one to approximate the expression for a single impurity at zero temperature [37]

$$G = G_0 \sin^2(\pi \langle n_k \rangle / 2), \tag{87}$$

where $\langle n_k \rangle$ is the bonding ($k = 0$) or antibonding ($k = \pi$) orbital occupancy. Expanding around the maximum we have $G(V_G) - G(V_G^{*,k}) \approx -G_0(\chi_c \pi/2)^2 (V_G - V_G^{*,k})$, where $V_G^{*,k}$ ($k = 0, \pi$) is the low/high voltage peak position and χ_c is the charge susceptibility, which may be approximated as $\chi_c \approx \partial \langle n_1 + n_2 \rangle / \partial V_G$, since the orbitals are filled separately. Values of the latter derivative read from figure 28(b) around the low and high voltage peak positions ($\langle n_1 + n_2 \rangle \approx 1$ and ≈ 3, respectively) provides a clear asymmetry. Moreover, the expansion of $G(V_G)$ allows one to roughly estimate the peak width as $\Delta V_G \approx \chi_c^{-1} \approx (U + K)/2 \sim \alpha$, which provides an indirect correspondence between the spectrum asymmetry and basis renormalization.

The practical possibility of the conductance measurement involving atom manipulation (changing of R) was also explored in terms of the system stability. Namely, the binding energies $\Delta E \equiv E_{R_{\min}} - E_\infty$ (where $R_{\min}$ is the bond length), listed in table 12, shows that the system becomes metastable around $V = 0.5t$ ($\Delta E > 0$ indicates a *local* energy minimum). Therefore, the binding of the atoms to the lead becomes stronger than interaction between the atoms, that may allow individual atom manipulation.

We would like to stress here that *ab initio* analysis have never been performed for the *open* system with strong electron correlation. Apart from simplifying the discussion (the model parameters are calculated as a function of interatomic distance), such an approach leads to new

physical effects, since the particle–hole symmetry is broken, as exemplified on the example of the conductivity calculations.

6. Concluding remarks

In this paper we have provided a detailed discussion of the method based on the diagonalization in the Fock space, when combined with with an *ab initio* adjustment of single-particle wavefunctions in the interacting state of the N-particle system (*the* EDABI *method*). The method can be improved upon by systematically increasing the number of wavefunctions in the basis $[w_i(\mathbf{r})]$ when defining the field operator for the system (thus enriching the model). We have illustrated our method with the discussion of several nanoscopic systems ranging from atoms to nanochains and quantum dots.

The method is useful when the exact solution of a model is available in the Fock space. Such a situation also occurs for the one-dimensional atomic chain represented by the Lieb–Wu solution of the Hubbard model [25]. In this situation, exact Wannier or Bloch wavefunctions can be constructed. Other applications such as solving the magnetic impurity in a nonmetallic environment are also possible, although not carried out explicitly as yet.

The importance of our approach is, among other things, in showing explicitly that the concept of the statistical distribution of particles with quasimomentum, as a good quantum number, is feasible for a relatively small interatomic distances. This means that the corresponding N-electron states form a quantum nanoliquid for not-too-large inter-distance in nanowires. In connection with this, in replying to the question of *how small a piece of metal can be*, we can say that the nanoliquid exhibits metallic conductivity for $eV \geqslant \Delta E(N, R)$, where V is the voltage applied to the system and $\Delta E(N, R)$ is the energy difference between the highest occupied and the lowest unoccupied state, i.e. the momentum is a good quantum number then. For an intermediate interatomic distace, we have a gradual transition to a Mott insulator, above which the monoatomic (quantum) nanowire is useless for electronic applications.

Acknowledgments

The authors were supported by the Ministry of Science and Higher Education, grant No 1P 03B 001 29. We also thank the Polish Science Foundation (FNP) for a Senior Fellowship (JS) and Foreign Postdoctoral Fellowship (AR). Discussions with Jan Kurzyk, Maciek Maśka, Robert Podsiadły and Włodek Wójcik were very important.

References

[1] cfe.g. Imry Y 2002 *Introduction to Mesoscopic Physics* (Oxford: Oxford University Press)
Heiss W D (ed) 2005 *Quantum Dots: a Doorway to Nanoscale Physics* (Berlin: Springer)
Jacak L, Hawrylak P and Wojs A 1998 *Quantum Dots* (Berlin: Springer)
[2] Spałek J, Podsiadły R, Wójcik W and Rycerz A 2000 *Phys. Rev.* B **61** 15676
Spałek J, Görlich E M, Rycerz A, Zahorbeński R and Wójcik W 2003 *Concepts in Electron Correlation* ed A C Hewson and V Zlatić (Dordrecht: Kluwer Academic) pp 257–68
[3] Slater J C 1963 *Quantum Theory of Molecules and Solids* vol 1 (New York: McGraw-Hill)
Korbel P, Wójcik W, Klejnberg A, Spałek J, Acquarone M and Lavagna M 2003 *Eur. Phys.* B **32** 315
[4] Rycerz A and Spałek J 2006 *Physica* B **378–80** 935
[5] Rycerz A 2003 *PhD Thesis* Jagiellonian University, Kraków (for online version see http://th-www.if.uj.edu.pl/ztms)
[6] Görlich E 2004 *PhD Thesis* Jagiellonian University, Kraków (for online version see http://th-www.if.uj.edu.pl/ztms)

[7] Zahorbeński R 2005 *PhD Thesis* Jagiellonian University, Kraków (for online version see http://th-www.if.uj.edu.pl/ztms)
[8] Spałek J, Datta A and Honig J M 1987 *Phys. Rev. Lett.* **59** 728
Spałek J, Datta A and Honig J M 1986 *Phys. Rev.* B **33** 4891
[9] Schweber S S 1961 *An Introduction to Relativistic Quantum Field Theory* (Evanston, IL: Row, Peterson and Co.) chapter 6
[10] Feynman RP 1972 *Statistical Mechanics: A Set of Lectures* (Menlo Park, CA: Benjamin) chapter 6.7
[11] Rycerz A and Spałek J 2001 *Phys. Rev.* B **63** 073101
Rycerz A and Spałek J 2002 *Phys. Rev.* B **65** 035110
For brief review see Spałek J, Rycerz A and Wójcik W 2001 *Acta Phys. Pol.* B **32** 3189
[12] Spałek J and Rycerz A 2001 *Phys. Rev.* B **64** 161105(R)
[13] Spałek J and Wójcik W 1992 *Phys. Rev.* B **45** 3799
Spałek J and Wójcik W 1992 *J. Magn. Magn. Mater.* **104–107** 723
Acquarone M, Iglesias J R, Gusmão M A, Noce C and Romano A 1998 *Phys. Rev.* B **58** 7626
Fortunelli A and Painelli A 1997 *J. Chem. Phys.* **106** 8041
[14] Shavitt R A 1977 *Methods of Electronic Structure Theory* ed H Schaeffer (New York: Plenum) pp 189–275
[15] Schrödinger E 1926 *Ann. Phys.* **79** 361
Cf Schrödinger E 1978 *Collected Papers on Wave Mechanics* (New York: Chelsea)
[16] Robertson B 1973 *Am. J. Phys.* **41** 678
[17] Mattis D C (ed) 1993 *The Many-Body Problem* (Singapore: World Scientific)
Korepin V E and Essler F H L 1994 *Exactly Solvable Models of Strongly Correlated Electrons* (River Edge, NJ: World Scientific)
[18] Szabo A and Ostlund N S 1996 *Quantum Chemistry* (Mineola: Dover)
[19] See e.g. Bethe H A and Salpeter E E 1957 *Quantum Mechanics of One-and Two-Electron Atoms* (New York: Academic) pp 146–156 and references therein
[20] Hubbard J 1964 *Proc. R. Soc.* A **281** 401
[21] Rycerz A and Spałek J 2006 *Phys. Status Solidi* b **243** 183
[22] Rycerz A and Spałek J 2004 *Eur. Phys. J.* B **40** 153
[23] Görlich E M, Kurzyk J, Rycerz A, Zahorbeński R, Podsiadły R, Wójcik W and Spałek J 2004 *Molecular Nanowires and Other Quantum Objects* ed A S Alexandrov, J Demsar and I K Yanson (Dordrecht: Kluwer) p 364
[24] Spałek J, Rycerz A, Görlich E M and Zahorbeński R 2003 *Highlights of Condensed Matter Physics (AIP Conf. Proc., New York)*; *AIP Conf. Proc.* **695** 291–303
[25] Lieb E H and Wu F Y 1968 *Phys. Rev. Lett.* **20** 1445
[26] Shastry B S and Sutherland B 1990 *Phys. Rev. Lett.* **65** 243
Millis J A and Coppersmith S N 1990 *Phys. Rev.* B **42** 10807
Góra D, Rościszewski K and Oleś A M 1998 *J. Phys.: Condens. Matter* **10** 4755
[27] Dagotto E 1994 *Rev. Mod. Phys.* **66** 763
Prelovšek P and Zotos X 2002 *Lectures on the Physics of Highly Correlated Electron Systems VI*; *AIP Conf. Proc.* **629** 161
[28] Davidson E R 1975 *J. Comput. Phys.* **17** 87
[29] Rycerz A and Spałek J 2004 *Eur. Phys. J.* B **40** 153
[30] Rycerz A and Spałek J 2006 *Phys. Status Solidi* b **243** 183
[31] Anderson P W 1959 *Phys. Rev.* **115** 2
Brinkman W F and Rice T M 1970 *Phys. Rev.* B **2** 1324
Chao K A, Spałek J and Oleś A M 1977 *J. Phys. C: Solid State Phys.* **10** L271
[32] Rejec T and Ramšak A 2003 *Phys. Rev.* B **68** 035342
Rejec T and Ramšak A 2003 *Phys. Rev.* B **68** 033306
[33] Anderson P W 1961 *Phys. Rev.* **124** 41
[34] Slater J C 1963 *Quantum Theory of Molecules and Solids* vol 1 (New York: McGraw-Hill) p 50
Spałek J *et al* 2000 *Phys. Rev.* B **61** 15676
[35] Kostyrko T and Bułka B 2003 *Phys. Rev.* B **67** 205331
[36] van der Wiel W G *et al* 2003 *Rev. Mod. Phys.* **75** 1
[37] Meir Y and Wingreen N S 1992 *Phys. Rev. Lett.* **68** 2512
Pastawski H M 1992 *Phys. Rev.* B **46** 4053
Jauho A-P, Wingreen N S and Meir Y 1994 *Phys. Rev.* B **50** 5528